Contemporary Mathematics
https://ojs.wiserpub.com/index.php/CM/

Research Article

Using Deep Neural Network and Fractional Derivative to Investigate Evolution of Virulence

Kamal Shah[1,2*], Aziz Khan[1], Thabet Abdeljawad[1], Eiman[2†]

[1] Department of Mathematics and Sciences, Prince Sultan University, Riyadh, 11586, Saudi Arabia
[2] Department of Mathematics, University of Malakand, Chakdara Dir(L), KPK, 18000, Pakistan
E-mail: kshah@psu.edu.sa; eiman@uom.edu.pk

Received: 14 December 2025; **Revised:** 27 January 2026; **Accepted:** 27 January 2026

Abstract: This manuscript is related to investigating a mathematical model for the evolution of virulence by using Deep Neural Networks (DNNs) and fractional order derivative with powerlaw kernel. Sufficient conditions are deduced for the existence and uniqueness of solution to the mentioned model. For the required results, fixed point theory is used. Also, some conditions related to local and global stability are established. Sensitivity analysis has also studied by using the direct method for the computed reproductive number. For the numerical analysis, we use the Euler's numerical tool. Further, DNNs is used to classify some probabilistic results including Mean Squared Error (MSE), Root Mean Squared Error (RMSE), and regression coefficient. We use the Levenberg-Marquardt algorithm to simulate the results. Several graphical illustrations have been given to to demonstrate the evolution process by using different values for fractional orders. Also, for all compartments, we have elaborated different graphical illustration to highlight the applicability of DNNs.

***Keywords*:** evolution of virus, neural network, fractional calculus, analysis, numerical analysis

MSC: 26A33, 34A08, 03C65

1. Introduction

Mathematical models are the powerful tools to study various real world problems. The idea of mathematical model was point out by Bernoulli's in 1776. Later on a formal mathematical model to address the epidemiological problem was given by Mekendrick and Karmark in 1927. With the help of mathematical models, we can understand the transmission dynamics of an infectious disease [1]. In the last century, significant contribution has been made by researchers in the field of mathematical epidemiology. In addition, physical and chemical as well as problems related to cosmology were investigated by using the concept of modeling. Infectious diseases have had a great impact on human life in history [2]. As various outbreaks due to viral infection have taken place in which millions of people have died. Some historical examples include Spanish influenza pandemic, first and second plague pandemic in Europe, Severe Acute Respiratory Syndrome (SARS), and Coronavirus Disease 2019 (COVID-19) in recent times [3]. Also, malaria has caused hundreds of millions of deaths throughout human history. For all mentioned diseases researchers have constructed mathematical models and they were studied comprehensively [4]. In recent times, mathematical models have implemented to addresses various real

DOI: https://doi.org/10.37256/cm.7220269389

world problems related to cyber security [5]. Turkyilmazoglu [6] studied solution of Susceptible-Infected-Recovered (SIR) and Susceptible-Exposed-Infected-Recovered (SEIR) type models. Turkyilmazoglu [7] studied an extended mathematical model with vaccination for weak immune system.

Due to selection of pressure in the environment, microorganism continually evolve. Pathogenic bacteria are frequently subject to selection pressure from antibiotics and the emergence of antibiotic resistant species poses a significant health challenge to medical research. Additionally, viruses directly compete with one another to reproduce, which leads to the evolution of virulence. Here, we investigate the potential evolution of virulence using the SIR endemic illness model. Consider a population which is initially in equilibrium in the presence of endemic disease due to wild type virus. Let the under the natural mutation process the virus mutates randomly. Now we want to investigate the conditions under what conditions the wild type virus be replaced by mutant virus in the population. The mentioned situation was formulated by Chasnov [8] and deduced how the mutant virus replace the wild type virus to maintain the equilibrium in the population. Let the original infected rate be β and the natural death rate of virus be μ and disease related death rate is δ. The corresponding rates for mutant virus can be represented by β', μ' and δ'. In addition, let assume that individual infected due to wild type or mutant virus gains immunity at the same time to both kind of viruses. Chasnov obtained the following formulation with two types of infections one denoted by I due to wild type virus and other I' due to mutant virus with one susceptible class S and the recovered class be R. The model is given by

$$\begin{aligned}
\dot{S}(t) &= \Lambda - dS - (\beta I + \beta' I')S, \ S(0) > 0, \\
\dot{I}(t) &= \beta SI - (r + d + c)I, \ I(0) \geq 0, \\
\dot{I}'(t) &= \beta' SI' - (r' + d + c')I', \ I'(0) \geq 0, \\
\dot{R}(t) &= rI + r'I' - dR, \ R(0) \geq 0.
\end{aligned} \tag{1}$$

A schematic diagram for model (1) is given in Figure 1.

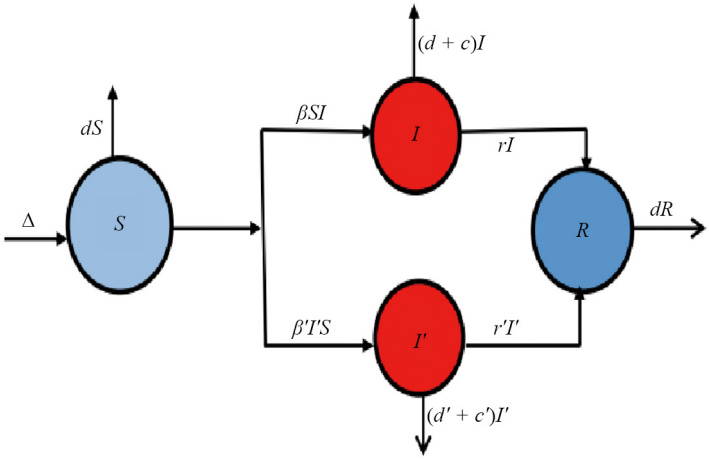

Figure 1. Schematic diagram of proposed model (1)

Recently, fractional calculus has received much attention from researchers. Because differential operators with fractional orders have the ability to describe dynamical behaviors of real world process with more comprehensive ways.

The concerned area has been utilized to investigate various real world applications. For instance, fractional calculus has been used to study epidemic models of infectious diseases [9] and [10]. The mentioned area has been used to study physical problems [11]. Also, in rheology and cosmology, fractional order derivatives were used to study related problems [12] and [13]. In biomedical engineering, the applications of fractional calculus can be easily read [14]. Researchers have extensively used differential and integral operators for investigating fluid mechanics problems very well [15] and [16]. Here, it is remarkable that there are numerous definitions for fractional derivatives which have been extensively used. These operators can be classified on the basis of kernel in two main types including singular and non-singular. Those differential operators involving power law kernels are considered singular operators like the Reimann-Liouville and Caputo operator [17]. On the other hand, those involve exponential or Mittag-Leffler kernel are called non singular differential operators [18]. Each operator has its own merits and demerits. The Liouville Caputo differential operator has been used by many researchers to investigate various real world problems [19]. Keeping in minds its merits like modeling real world problems with memory or nonlocal effects more excellently, we use this operator to investigate model (1). The extended form of model (1) becomes

$$\begin{aligned}
{}^{C}D_t^p S(t) &= \Lambda - dS - (\beta I + \beta' I')S, \;\; S(0) > 0,\\
{}^{C}D_t^p I(t)(t) &= \beta SI - (r + d + c)I, \;\; I(0) \geq 0,\\
{}^{C}D_t^p I'(t) &= \beta' SI' - (r' + d + c')I', \;\; I'(0) \geq 0,\\
{}^{C}D_t^p R(t)(t) &= rI + r' I' - dR, \;\; R(0) \geq 0,
\end{aligned} \tag{2}$$

where p is the fractional order $0 < p \leq 1$ and ${}^{C}D_t^p$ is Liouville-Caputo derivative [20] defined for a function $g \in C[0, T]$ as

$${}^{C}D_t^p g(t) = \frac{1}{\Gamma(1-p)} \int_0^t (t-\omega)^{-p} g'(\omega) d\omega.$$

Also, the Riemann-Liouville integral operator for $p > 0$ is defined by

$$I_t^p g(t) = \frac{1}{\Gamma(p)} \int_0^t (t-\omega)^{p-1} g'(\omega) d\omega.$$

Also, the following relation holds

$${}^{C}D_t^p [I_t^p g(t)] = g(t).$$

Further, one has for $0 < p \leq 1$, that

$$I_t^p [{}^{C}D_t^p g(t)] = g(t) - C_0,$$

where C_0 is a real constant. We study the positivity and boundedness of model (2). Also, the existence theory together with numerical analysis has been investigated by using the Runge-Kutta method of order 4 (RK4). For existence theory fixed point tools have been utilized.

In recent time, Artificial Intelligence (AI) based tools like Artificial Neural Networks (ANNs) and Deep Neural Networks (DNNs) have attracted the attention from researchers very well. Here, we note that ANNs are computer programs designed to mimic biological processes and then train to process information similarly to the human brain. There are numerous ANN tools available, some of which are well-known, such as Neural Networks (NN) and DNN tools. The use of the aforementioned AI technologies has been the subject of numerous types of research recently. Here, we highlighted the work of scholars [21] who have provided comprehensive details on the fundamentals of AI tools. Auto progressive training of NNs constitutive models has been studied in depth by researchers [22]. Authors [23] have used DNNs to investigate infectious disease model of COVID-19. However, DNN-based AI models and differential equation-based epidemic compartmental models have recently studied in many research works, we refer to [24, 25]. For example, in AI models, the biological pattern is not explained, whereas in compartmental models, parameter estimation is limited. Nonetheless, AI models are being used more and more as effective instruments for examining epidemic simulations. Here, we demonstrate that the large scale networks needed for deep learning can now be trained because to recent advancements in processing power, particularly specialized hardware like Graphics Processing Units (GPUs) and Tensor Processing Units (TPUs), and the abundance of training data. These developments have made it possible for DNNs to transition from theoretical models to useful real-world applications. Researchers [26] have used AI tools to investigate Human Immunodeficiency Virus/Acquired Immunodeficiency Syndrome (HIV/AIDS) disease model. Also, Uranium decay process and Zika virus disease was studied by using AI based NNs recently in [27] and [28]. DNNs are consisted on multi hidden layers between input and output layers which learn complex features and pattern from the data through input and processes for various applications. Also, in simple words, a DNN is a function which take input say x and process them to produce out put y. We define the processes as follows [29]:

$$Gu = v,\ u \in R^m,\ v \in R^n,$$

where m, n are dimensions of input and output respectively. An input $u \in R^m$ is feed to DNN which produce output $v \in R^n$. The process is expressed mathematically as follows:

$$v = \mu_a(Wu + b),\ W \in R^{m\times n},\ b \in R^n,$$

here μ_a stands for activation function. A DNN with four inputs which processes through multiple hidden layers to create out put can be diagrammatically described as in Figure 2.

Here, we remark that recently, researchers have used the AI based NNs to investigate various dynamical problems, we refer few to [30–32]. With the help of DNNs, we investigate the model (2) and classify various results including Root Mean Squared Error (RMSE), Mean Squared Error (MSE), and regression coefficient etc for all data, validation of data, test and train data. The mentioned results are displayed graphically by using Matlab 2023 following the Levenberg-Marquardt algorithm. From the above discussion, we found that DNNs together with fractional derivative have not used to investigate the mathematical model of evolution of viruses in a community. Because mutation of viruses is a serious problem during the spread of infectious diseases. For instance during COVID-19, various form of viruses appeared which caused new wave of infection due to mutation. Therefore, to fill this gap we have conducted this research on evolution of viruses to understand the procedure which will help researchers in further research on mentioned area.

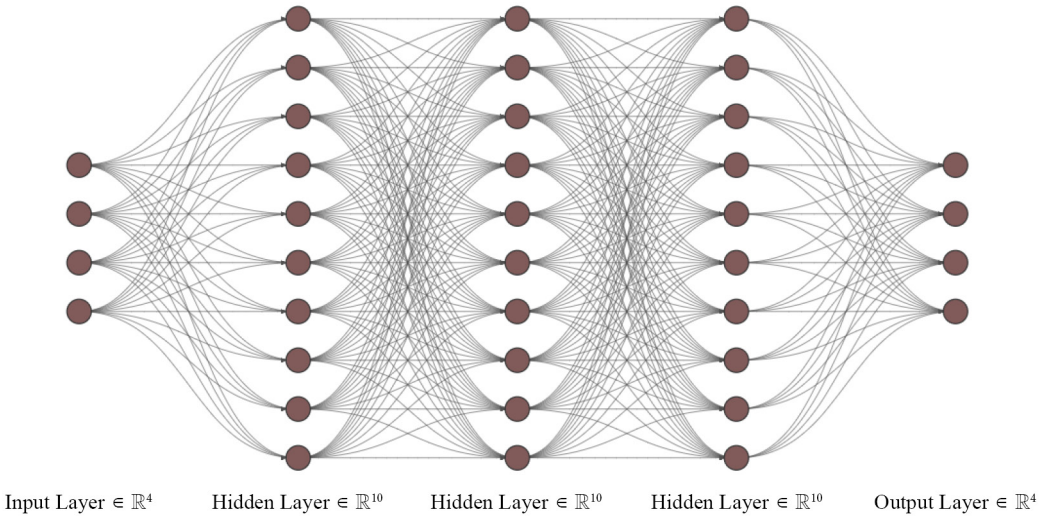

Figure 2. Diagram of DNN

2. Fundamental results related to model (2)

Some fundamental results on positivity and boundedness have given in Appendix A. Now, we compute the equilibrium points. If the population is in equilibrium with both types of viruses, that is $I = 0$, $I' = 0$, then $S = \frac{\Lambda}{d}$ and $R = 0$. Therefore, disease free equilibrium point is $E_0 = \left(\frac{\Lambda}{d}, 0, 0, 0\right)$. Further, let the population is in equilibrium with wild type of virus, then $I = 0$, $I' \neq 0$, and

$$S^* = \frac{r'+d+c'}{\beta'},\ I'^* = \frac{\beta'\Lambda - d(r'+d+c')}{\beta'(r'+d+c')},\ R^* = \frac{r'}{d}\left[\frac{\beta'\Lambda - d(r'+d+c')}{\beta'(r'+d+c')}\right].$$

On the other hand if population is in equilibrium corresponding to virus I, that is $I' = 0$, $I \neq 0$, then the corresponding equilibrium points are given by

$$S_* = \frac{r+d+c}{\beta},\ I_* = \frac{\beta\Lambda - d(r+d+c)}{\beta(r+d+c)},\ R_* = \frac{r}{d}\left[\frac{\beta\Lambda - d(r+d+c)}{\beta(r+d+c)}\right].$$

To compute the reproductive number (numbers), we proceed as follows.
From third and second equations of model (2), we have

$$^{C}D_t^p I'(t) = \beta' SI' - (r'+d+c')I'.$$

$$^{C}D_t^p I(t)(t) = \beta SI - (r+d+c)I. \tag{3}$$

We see from (3),

$$f = \begin{pmatrix} \beta' SI' \\ \\ \beta SI \end{pmatrix}, \; v = \begin{pmatrix} -(r'+d+c')I' \\ \\ -(r+d+c)I \end{pmatrix}.$$

The Jacobian matrices of f, v at disease free equilibrium are computed as follows:

$$F = \begin{pmatrix} \frac{\beta'\Lambda}{d} & 0 \\ \\ 0 & \frac{\beta\Lambda}{d} \end{pmatrix}, \; V^{-1} = \begin{pmatrix} \frac{-1}{(r+d+c)} & 0 \\ \\ 0 & \frac{-1}{(r'+d+c')} \end{pmatrix}.$$

Hence, we have

$$FV^{-1} = \begin{pmatrix} \frac{\beta'\Lambda}{d(r+d+c)} & 0 \\ \\ 0 & \frac{\beta\Lambda}{d(r'+d+c')} \end{pmatrix}.$$

Therefore, the basic reproductive number is given by

$$\mathscr{R}_{1,0} = \frac{\beta'\Lambda}{d(r+d+c)}, \text{ or } \mathscr{R}_{2,0} = \frac{\beta\Lambda}{d(r'+d+c')}.$$

We do some analysis, by using $S = S_*$, we have from second equation of model (2)

$${}^{C}D_t^p I'(t)(t) = \left[\beta' \frac{r+d+c}{\beta} - (r'+d+c')\right] I.$$

We see that I' is increases if $\beta' \frac{(r+d+c)}{\beta} - (r'+d+c') > 0$ that is

$$\frac{\beta}{(r+d+c)} < \frac{\beta'}{(r'+d+c')}$$

which shows that endemic viruses will goes to evolve when $\beta' > \beta$, and infection will survive more rapidly if $r' < r$. Also, dead ratio will be less if $c' < c$. In the same way, if we replace $S = S^*$ in second equation

$${}^{C}D_t^p I'(t) = \beta' SI' - (r'+d+c')I',$$

we have $\frac{\beta}{(r+d+c)} > \frac{\beta'}{(r'+d+c')}$. In this case $\beta > \beta'$, $r < r'$ and $c < c'$.

Theorem 1 The disease free equilibrium is locally asymptotically stable if $\mathscr{R}_{1,0} < 1$, $\mathscr{R}_{2,0} < 1$.

Proof. The Jacobian matrix of model (2) at disease free equilibrium is given by

$$J_{E_0} = \begin{pmatrix} -d & \frac{-\beta\Lambda}{d} & \frac{-\beta'\Lambda}{d} & 0 \\ 0 & \frac{\beta\Lambda}{d} - (r+d+c) & 0 & 0 \\ 0 & 0 & \frac{\beta'\Lambda}{d} - (r'+d+c') & 0 \\ 0 & r & r' & -d \end{pmatrix}. \tag{4}$$

Then, we have

$$\det[J_{E_0} - \lambda \mathbf{I}] = 0, \tag{5}$$

where $\mathbf{I}$ is identity matrix of order 4×4. We get

$$\lambda_1 = -d,\ \lambda_2 = \frac{\beta\Lambda}{d} - (r+d+c),\ \lambda_3 = \frac{\beta'\Lambda}{d} - (r'+d+c'),\ \lambda_4 = -d.$$

Since, λ_1, λ_4 have negative real parts, while from $\lambda_2 = (r+d+c)\left[\frac{\beta\Lambda}{d(r+d+c)} - 1\right] = (r+d+c)\left[\mathscr{R}_{1,0} - 1\right]$, and $\lambda_3 = (r'+d+c')\left[\frac{\beta'\Lambda}{d(r'+d+c')} - 1\right] = (r'+d+c')\left[\mathscr{R}_{2,0} - 1\right]$, we see that λ_2, λ_3 have negative real parts if $\mathscr{R}_{1,0} < 1, \mathscr{R}_{2,0} < 1$. Thus proved. □

Sensitivity analysis is an important tool to determine how much the impact be produced by varying the parameters in the reproductive number. For the computation of sensitivity analysis, three methods are usually used including direct method [33], the method given by Chitnis et al. [34] by linearizing the model (1) and Latin hypercube sampling technique [35]. Here, we follow the direct method based on the following formula with respect to the parameters q:

$$\$_q^{\mathscr{R}_{i,0}} = q\frac{\partial}{\partial q}\log|\mathscr{R}_{i,0}|,\ i = 1, 2.$$

Hence, we have by using the given values for parameters $\Lambda = 0.01456$; $\beta' = 0.01234$; $d' = 0.00000139$; $r' = 0.0019$; $c' = 0.09$.

$$\$_{\beta'}^{\mathscr{R}_{1,0}} = \beta'\frac{\partial}{\partial\beta'}\log\left|\frac{\beta'\Lambda}{d(r+d+c)}\right| = 1 > 0,$$

$$\$_{\Lambda}^{\mathscr{R}_{1,0}} = \Lambda\frac{\partial}{\partial\Lambda}\log\left|\frac{\beta'\Lambda}{d(r+d+c)}\right| = 1 > 0,$$

$$\$_{d'}^{\mathscr{R}_{1,0}} = d\frac{\partial}{\partial d}\log\left|\frac{\beta'\Lambda}{d(r+d+c)}\right| = \frac{-(2d+r+c)}{r+d+c} = -1.00000136406 < 0,$$

$$\$_{r'}^{\mathscr{R}_{1,0}} = r\frac{\partial}{\partial r}\log\left|\frac{\beta'\Lambda}{d(r+d+c)}\right| = \frac{-r}{r+d+c} = -0.0186454768 < 0,$$

$$\$_{c'}^{\mathscr{R}_{1,0}} = c\frac{\partial}{\partial c}\log\left|\frac{\beta'\Lambda}{d(r+d+c)}\right| = \frac{-c}{r+d+c} = -0.9813408826 < 0.$$

In the same way, we can find for the other reproductive number by using values of parameters as $\Lambda = 0.01456$; $\beta = 0.0533$; $d = 0.00000139$; $r = 0.0035$; $c = 0.1$.

$$\$_{\beta}^{\mathscr{R}_{2,0}} = \beta\frac{\partial}{\partial \beta}\log\left|\frac{\beta\Lambda}{d(r'+d+c')}\right| = 1 > 0,$$

$$\$_{\Lambda}^{\mathscr{R}_{2,0}} = \Lambda\frac{\partial}{\partial \Lambda}\log\left|\frac{\beta'\Lambda}{d(r'+d+c')}\right| = 1 > 0,$$

$$\$_{d}^{\mathscr{R}_{2,0}} = d\frac{\partial}{\partial d}\log\left|\frac{\beta\Lambda}{d(r'+d+c')}\right| = \frac{-(2d+r'+c')}{r'+d+c'} = -1.0000148661,$$

$$\$_{r}^{\mathscr{R}_{2,0}} = r'\frac{\partial}{\partial r'}\log\left|\frac{\beta\Lambda}{d(r'+d+c;)}\right| = \frac{-r'}{r'+d+c'} = -0.0374325986,$$

$$\$_{c}^{\mathscr{R}_{2,0}} = c'\frac{\partial}{\partial c'}\log\left|\frac{\beta\Lambda}{d(r'+d+c')}\right| = \frac{-c'}{r'+d+c'} = -1.069502817 < 0.$$

From the sensitivity relation, we see that 100% increase in the values of Λ, β, β' will produce 100% increase in the values of $\mathscr{R}_{i,0}$, $i = 1, 2$. In the same process 100% decrease in the values of d causes 100% decrease in the values of $\mathscr{R}_{i,0}$, $i = 1, 2$. Also, if we decrease 100% the values of r, r' which will cause 1% and 3% decrease in the values of $\mathscr{R}_{i,0}$, $i = 1, 2$. But the 100% decrease in values of c, c' cause 98% and 100% decrease in the values of $\mathscr{R}_{i,0}$, $i = 1, 2$. These demonstrate that Λ, β, β', c, c' are the most sensitive parameters.

2.1 *Some qualitative results*

To establish some qualitative results, let define a Banach space $\mathbb{X} = C[0, T] \times C[0, T] \times C[0, T] \times C[0, T]$ with norm

$$\|\phi\| = \max_{t\in[0,T]} |\phi(t)|, \text{ where } \phi = (S, I, I', R).$$

In addition, we write the model (2) as follows:

$$\begin{cases} {}^{C}D_t^p \phi(t) = \mathscr{F}(t, \phi(t)), \\ \\ \phi(0) = \phi_0, \end{cases} \tag{6}$$

where

$$\mathscr{F}(t,\phi(t))=\begin{pmatrix}\Lambda-dS-(\beta I+\beta' I')S\\ \beta SI-(r+d+c)I\\ \beta' SI'-(r'+d+c')I'\\ rI+r'I'-dR,\end{pmatrix},$$

and $\phi_0=(S_0, I_0, I_0', R_0)$.

Then system (13) is equivalent to the integral equations given by

$$\phi(t)=\phi_0+\frac{1}{\Gamma(p)}\int_0^t(t-\omega)^{p-1}\mathscr{F}(\omega,\phi(\omega))d\omega. \tag{7}$$

Further, we state some data dependence results as:

(H_1) For constants $C_{\mathscr{F}}>0$, and $D_{\mathscr{F}}>0$, we have

$$|\mathscr{F}(t,\phi(t))|\leq C_{\mathscr{F}}|\phi|+D_{\mathscr{F}}.$$

(H_2) For real value $L_{\mathscr{F}}>0$, and $\phi, \bar{\phi}\in\mathbb{X}$, one has

$$\left|\mathscr{F}(t,\phi(t))-\mathscr{F}(t,\bar{\phi}(t))\right|\leq L_{\mathscr{F}}\left|\phi-\bar{\phi}\right|.$$

Theorem 2 The model (2) has at least one solution under the assumption (H_1) and if $\frac{C_{\mathscr{F}}T^p}{\Gamma(p+1)}<1$. In addition, if the condition $\frac{T^pL_{\mathscr{F}}}{\Gamma(p+1)}<1$ holds, then the mentioned model has a unique solution.

Proof. Let us define a closed bounded set Q of $\mathbb{X}$, such that

$$\{\phi\in\mathbb{X}\colon\|\phi\|\leq\rho\},$$

where $r\geq\frac{|\phi_0|+\frac{D_{\mathscr{F}}T^p}{\Gamma(p+1)}}{1-\frac{C_{\mathscr{F}}T^p}{\Gamma(p+1)}}$. In addition if $\mathbb{P}\colon Q\to\mathbb{X}$ is defined by

$$\mathbb{P}(\phi)=\phi_0+\frac{1}{\Gamma(p)}\int_0^t(t-\omega)^{p-1}\mathscr{F}(\omega,\phi(\omega))d\omega \tag{8}$$

Since $\mathscr{F}$ is continuous, therefore, the operator $\mathbb{P}$ is also continuous. Now we show that $\mathbb{P}$ is bounded. Let take $\phi\in Q$, and consider

$$
\begin{aligned}
|\mathbb{P}(\phi)| &= \left|\phi_0 + \frac{1}{\Gamma(p)}\int_0^t (t-\omega)^{p-1}\mathscr{F}(\omega, \phi(\omega))d\omega\right| \\
&\leq |\phi_0| + \frac{1}{\Gamma(p)}\int_0^t (t-\omega)^{p-1}|\mathscr{F}(\omega, \phi(\omega))d\omega| \\
&\leq |\phi_0| + \frac{1}{\Gamma(p)}\int_0^t (t-\omega)^{p-1}[C_{\mathscr{F}}|\phi(\omega)| + D_{\mathscr{F}}]d\omega \\
&\leq |\phi_0| + \frac{[C_{\mathscr{F}}\rho + D_{\mathscr{F}}]}{\Gamma(p)}\int_0^t (t-\omega)^{p-1}d\omega \\
&= |\phi_0| + \frac{[C_{\mathscr{F}}\rho + D_{\mathscr{F}}]T^p}{\Gamma(p+1)} \\
&\leq \rho,
\end{aligned}
$$

which shows that $|\mathbb{P}(\phi)| \leq \rho$. Hence $\mathbb{P}$ is bounded also continuous so is uniformly continuous. Therefore, $\|\mathbb{P}(\phi)\| \leq \rho$ implies that $\mathbb{P}$ maps bounded set to bounded. Next we prove that $\mathbb{P}$ is equi-continuous. Let $t < \tau$, and consider

$$
\begin{aligned}
|\mathbb{P}(\phi)(\tau) - \mathbb{P}(\phi)(t)| &= \left|\frac{1}{\Gamma(p)}\int_0^\tau (\tau-\omega)^{p-1}\mathscr{F}(\omega, \phi(\omega))d\omega - \frac{1}{\Gamma(p)}\int_0^t (t-\omega)^{p-1}\mathscr{F}(\omega, \phi(\omega))d\omega\right| \\
&\leq \frac{1}{\Gamma(p)}\int_0^t [(\tau-\omega)^{p-1} - (t-\omega)^{p-1}]|\mathscr{F}(\omega, \phi(\omega))|d\omega + \frac{1}{\Gamma(p)}\int_t^\tau (\tau-\omega)^{p-1}|\mathscr{F}(\omega, \phi(\omega))|d\omega \\
&\leq \frac{1}{\Gamma(p)}(C_{\mathscr{F}}\rho + D_{\mathscr{F}})\left[\int_0^t [(\tau-\omega)^{p-1} - (t-\omega)^{p-1}]d\omega + \int_t^\tau (\tau-\omega)^{p-1}d\omega\right] \\
&= \frac{(C_{\mathscr{F}}\rho + D_{\mathscr{F}})}{\Gamma(p+1)}[\tau^p - t^p]\,d\omega. \qquad (9)
\end{aligned}
$$

The right side of (9) becomes zero at $t \to \tau$. Hence left side is also becomes zero at $t \to \tau$. Since $\mathbb{P}$ is uniformly continuous, therefore at $t \to \tau$, we get

$$
\|\mathbb{P}(\phi)(\tau) - \mathbb{P}(\phi)(t)\| \to 0
$$

which demonstrate that $\mathbb{P}$ is equi-continuous. Hence $\mathbb{P}$ is completely continuous. In view of Schauder's fixed theorem [36], the model (2) has at least one solution. Further, let ϕ, $\bar{\phi} \in \mathbb{X}$, taking

$$\|\mathbb{P}(\phi)-\mathbb{P}(\bar{\phi})\| = \max_{t\in[0,T]}\left|\frac{1}{\Gamma(p)}\int_0^t (t-\omega)^{p-1}\mathscr{F}(\omega,\phi(\omega))d\omega - \frac{1}{\Gamma(p)}\int_0^t (t-\omega)^{p-1}\mathscr{F}(\omega,\bar{\phi}(\omega))d\omega\right|$$

$$\leq \max_{t\in[0,T]}\frac{1}{\Gamma(p)}\int_0^t (t-\omega)^{p-1}\left|\mathscr{F}(\omega,\phi(\omega))-\mathscr{F}(\omega,\bar{\phi}(\omega))\right|d\omega$$

$$\leq \frac{T^p L_{\mathscr{F}}}{\Gamma(p+1)}\left\|\phi-\bar{\phi}\right\|,$$

which shows that $\mathbb{P}$ is a contraction operator and hence model (2) has a unique solution. □

Researchers have extensively established the Lyapunov stability theory for fractional derivatives. For these purposes, they have extended the classical stability theory to systems described by fractional differential equations. Numerous theoretical results have been established on the mentioned topic. Here, we follow the results deduced by authors [37] to construct some results for the proposed model.

Theorem 3 The disease free equilibrium is globally asymptotically stable of model (2) if $\Lambda < dN + cI + c'I'$.

Proof. Consider a Lyapunov function described by

$$\Psi(t,S,I,I',R) = a_1(S-S_0)+a_2(I-I_0)+a_3(I'-I_0')+a_4(R-R_0), \tag{10}$$

where a_i, $i=1,2,3,4$ are real values to be determined later. We follow [37] to conduct stability result. Applying derivative to (10), we have

$$\begin{aligned}{}^{C}D_t^p\Psi(t,S,I,I',R) =& a_1\,{}^{C}D_t^p S(t)+a_2\,{}^{C}D_t^p I(t)+a_3\,{}^{C}D_t^p I'(t)+a_4\,{}^{C}D_t^p R(t)\\ =& a_1[\Lambda-dS-(\beta SI+\beta' SI')]+a_2[\beta SI-(r+d+c)I]\\ &+a_3[\beta' SI'-(r'+d+c')I']+a_4[rI+r'I'-dR].\end{aligned} \tag{11}$$

Setting $a_i=1$, $\forall\, i=1,2,3,4$, we have from (11)

$${}^{C}D_t^p\Psi(t,S,I,I',R) = \Lambda-dN-cI-c'I'<0.$$

Hence ${}^{C}D_t^p\Psi(t,S,I,I',R)<0$, while $\Psi(t,.,.,.,.)\geq 0$. Thus Ψ is negative definite. Thus the disease free equilibrium is globally asymptotically stable. □

3. Numerical interpretation

Here, we deduce the numerical scheme for the concerned model. We write the model (2) as bellow:

$$
\begin{aligned}
{}^{C}D_t^p S(t) &= \Lambda - dS - (\beta I + \beta' I')S = \mathscr{F}_1(t, S, I, I', R),\\
{}^{C}D_t^p I(t) &= \beta SI - (r + d + c)I = \mathscr{F}_2(t, S, I, I', R),\\
{}^{C}D_t^p I'(t) &= \beta' SI' - (r' + d + c')I' = \mathscr{F}_3(t, S, I, I', R),\\
{}^{C}D_t^p R(t) &= rI + r'I' - dR = \mathscr{F}_4(t, S, I, I', R).
\end{aligned} \tag{12}
$$

We divide the interval of solution $[0,\ T]$ in to m sub interval $[t_j,\ t_{j+1}]$ with uniform width of $h = \frac{T-0}{m}$, $j = 0,\ 1,\ 2,\ ...,\ m-1$, and $t_j = jh$. Let $S(t)$, $I(t)$, $I'(t)$, $R(t)$, ${}^{C}D_t^p S(t)$, ${}^{C}D_t^p I(t)$, ${}^{C}D_t^p I'(t)$, ${}^{C}D_t^p R(t)$ are continuous, then using $t_0 = 0$ and apply Taylor formula to the considered model in the form of (13) by ignoring higher power of h that is h^{2p}, etc, we get [38]

$$
\begin{aligned}
S(t_{j+1}) &= S(t_j) + \frac{h^p}{\Gamma(p+1)}\mathscr{F}_1(t_j, S(t_j), I(t_j), I'(t_j), R(t_j)),\\
I(t_{j+1}) &= I(t_j) + \frac{h^p}{\Gamma(p+1)}\mathscr{F}_2(t_j, S(t_j), I(t_j), I'(t_j), R(t_j)),\\
I'(t_{j+1}) &= I'(t_j) + \frac{h^p}{\Gamma(p+1)}\mathscr{F}_3(t_j, S(t_j), I(t_j), I'(t_j), R(t_j)),\\
R(t_{j+1}) &= R(t_j) + \frac{h^p}{\Gamma(p+1)}\mathscr{F}_4(t_j, S(t_j), I(t_j), I'(t_j), R(t_j)),
\end{aligned} \tag{13}
$$

for $j = 0,\ 1,\ 2,\ ...,\ m-1$. We use $(S(0),\ I(0),\ I'(0),\ R(0)) = (10,\ 4,\ 3,\ 1)$, and the parameters values were selected as $\Lambda = 0.01456$; $\beta = 0.0533$; $\beta' = 0.01234$; $d = 0.00000139$; $r = 0.0019$; $r' = 0.0035$; $c = 0.1$; $c' = 0.09$. We present the numerical results graphically by using various fractional orders in Figures 3, 4.

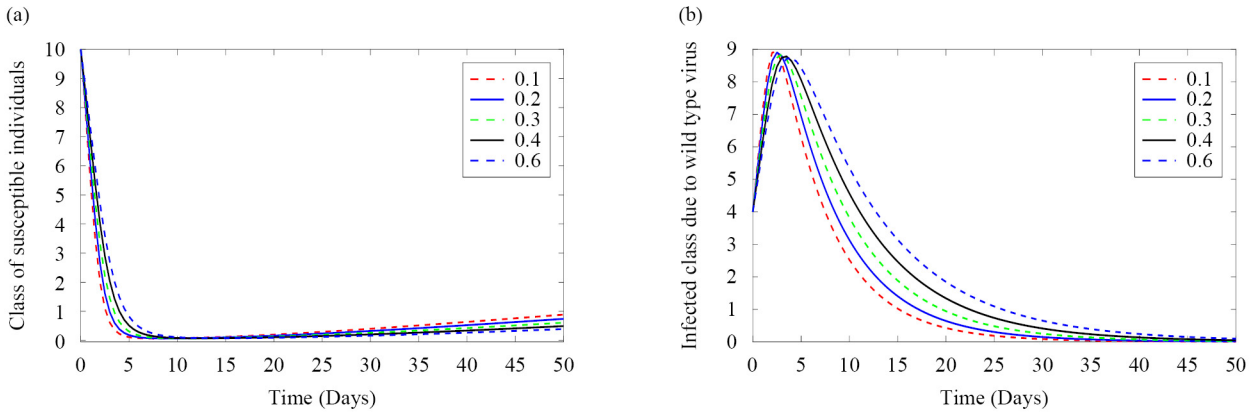

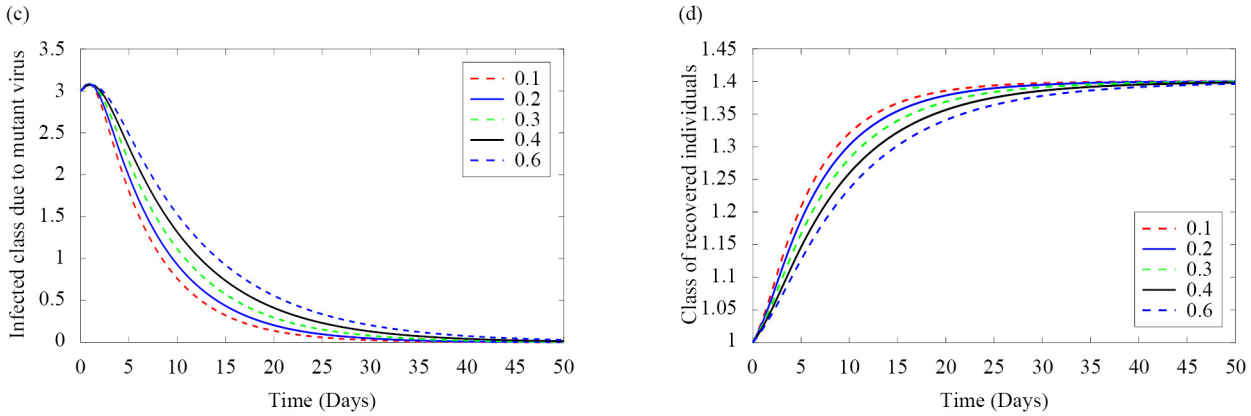

Figure 3. Graphical illustrations for various compartments of model (2) using various fractional orders in $(0, 0.5]$. (a) susceptible individuals class (b) infected class due to wild type virus (c) infected class due to mutant virus (d) recovered individuals

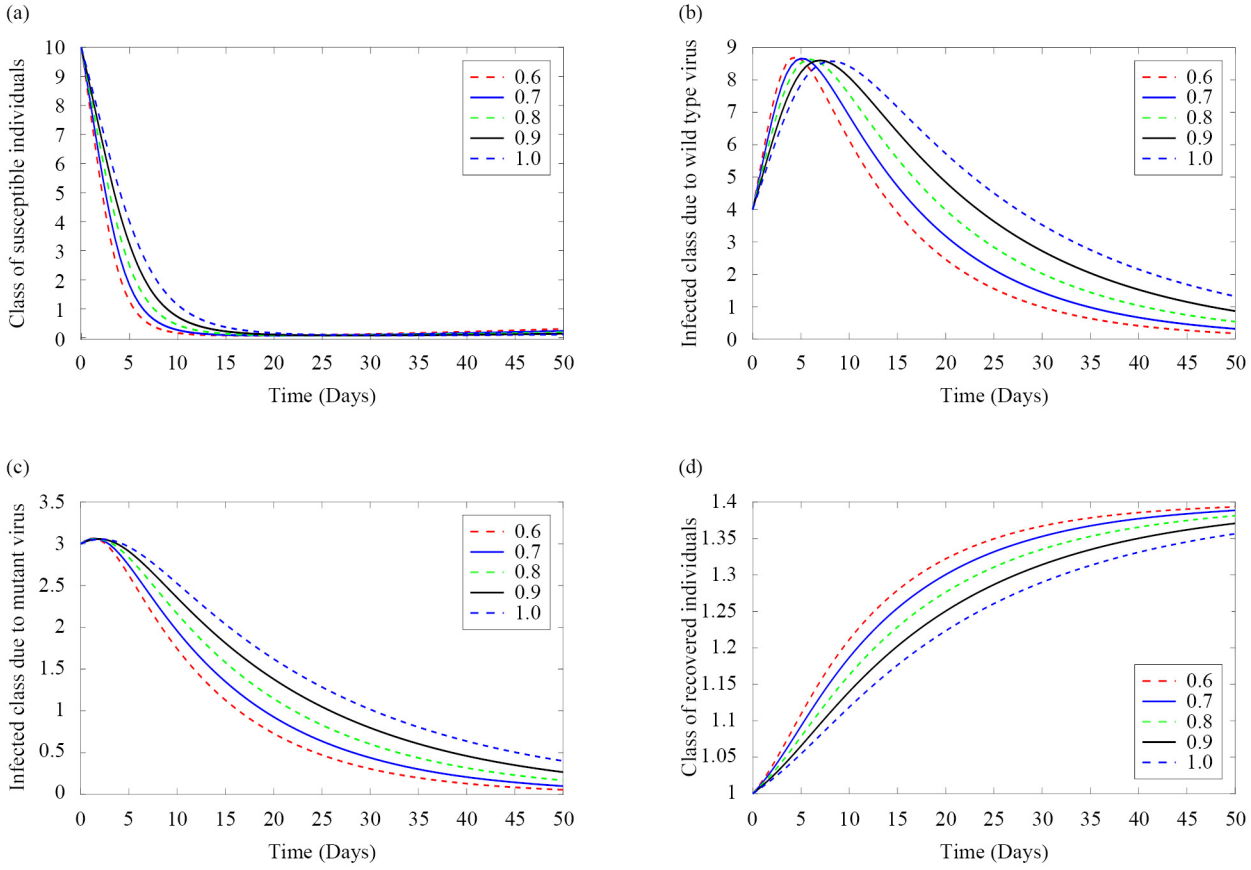

Figure 4. Graphical illustrations for various compartments of model (2) using various fractional orders in $(0.5, 1.0]$. (a) susceptible individuals class (b) infected class due to wild type virus (c) infected class due to mutant virus (d) recovered individuals

3.1 *DNNs analysis of model (2)*

In this part, we perform the computational analysis based on DNNs following the Levenberg-Marquardt algorithm. We compute MSE, RMSE and regression coefficient for each class and compute it graphically. For the mentioned quantities, we use the following formulae:

$$\text{MSE} = \sum_{i=1}^{n} \frac{|\hat{\text{X}}_i - \text{X}_i|^2}{X_i}, \ \mu = \sum_{i=1}^{n} \frac{[\hat{\text{X}}_i - \text{X}_i]^2}{n-1},$$

$$\text{RMSE} = \sum_{i=1}^{n} \frac{|\hat{\text{X}}_i - \text{X}_i|^2}{n}, \ \sigma = \sqrt{\sum_{i=1}^{n} \frac{[\hat{\text{X}}_i - \text{X}_i]^2}{n-1}}.$$

Further, the structure of the DNN can be presented graphically with hidden layers in Figure 5.

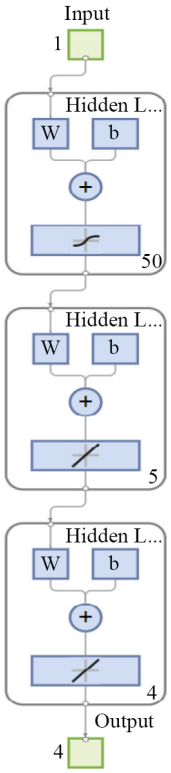

Figure 5. DNN structure

The best validation performance is achieved for class S is $2.8625e-08$ at epoch 1,000. We use total of 38 neuron, maximum epoch upto 1,000 and the activation function $a_c = \tanh x$. We have presented in Figures 6, 7, 8, and 9 each compartments details respectively. In Figure 6, we have presented the results graphically. In sub Figure 6 (a), we have presented the MSE $= 1.6988e-06$, RMSE $= 0.0013034$ and here the regression coefficient is 1 which shows the accuracy of our simulation. In the same way, in sub Figure 6 (b), the train data has been tested, where MSE $= 1.6798e-06$, RMSE $=$ 0.0012961. Also, in sub Figure 6 (c), and sub Figure 6 (d), we have presented the validation and test data for the class S. Here, MSE $= 1.7782e-06$, RMSE $= 0.0013335$ and MSE $= 1.708e-06$, RMSE $= 0.0013069$ respectively represents the respective errors analysis of validation and test data. In sub Figures 6 (e), (f), (g) and (h), we have demonstrated the graphical presentations of absolute error analysis, comparison, performance and best function fit for class S. The maximum absolute error is bounded by 10^{-2}.

(a)

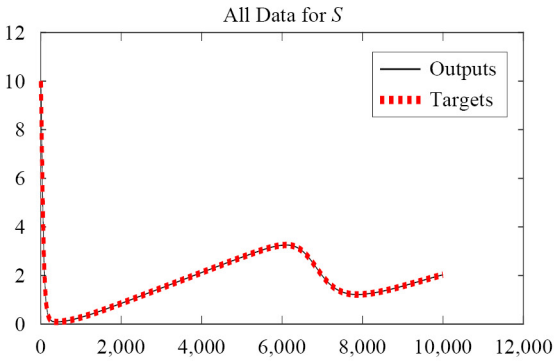
All Data for S
Outputs
Targets

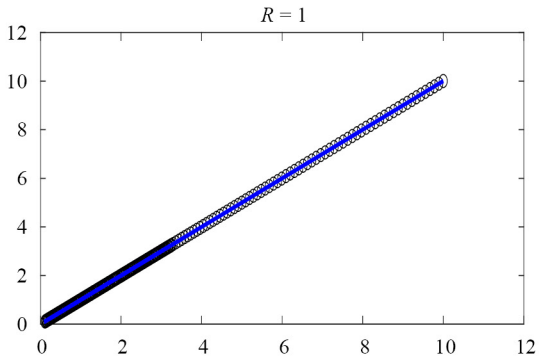
R = 1

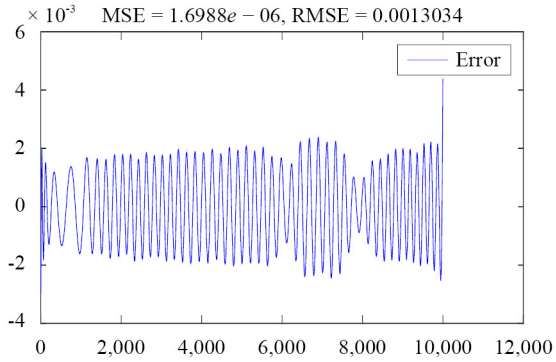
× 10-3 MSE = 1.6988e − 06, RMSE = 0.0013034
Error

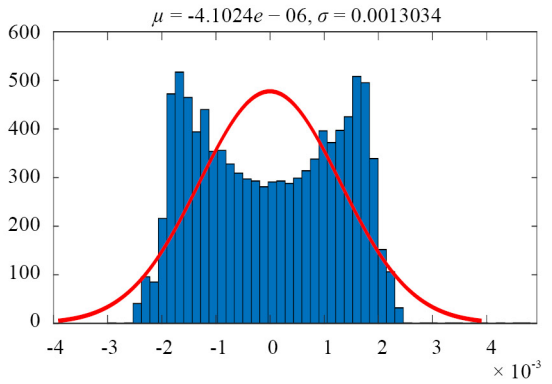
μ = -4.1024e − 06, σ = 0.0013034
× 10-3

(b)

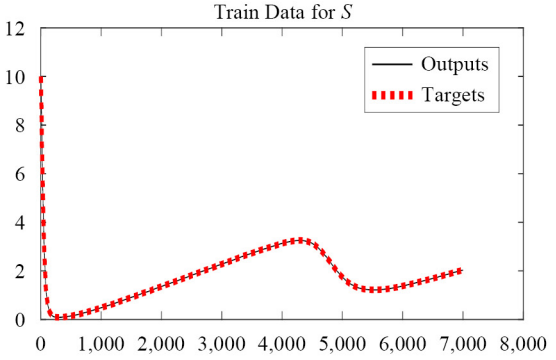
Train Data for S
Outputs
Targets

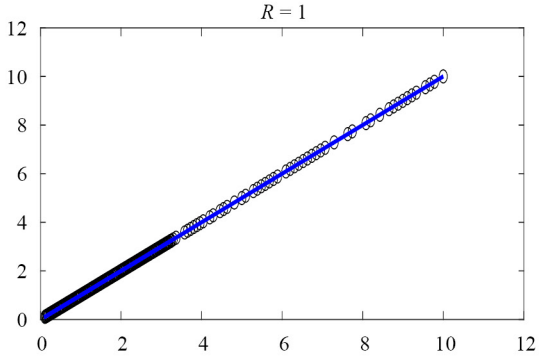
R = 1

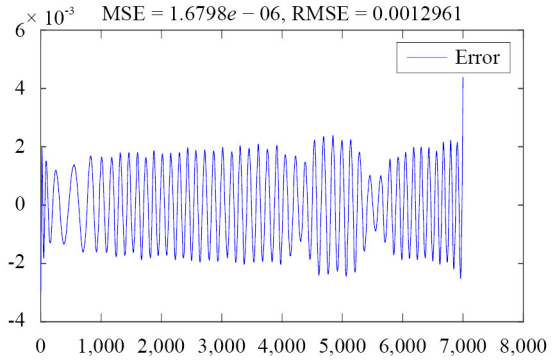
× 10-3 MSE = 1.6798e − 06, RMSE = 0.0012961
Error

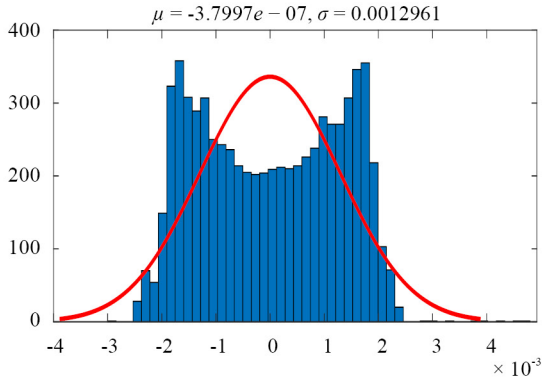
μ = -3.7997e − 07, σ = 0.0012961
× 10-3

(c)

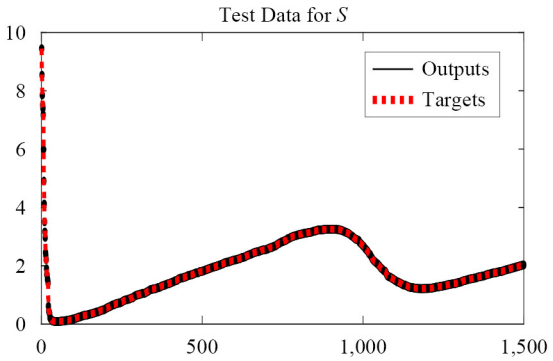
Test Data for S
Outputs
Targets

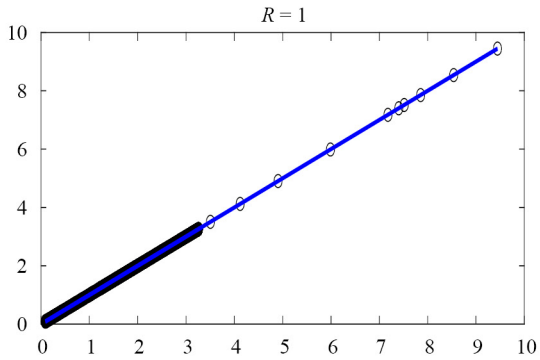
R = 1

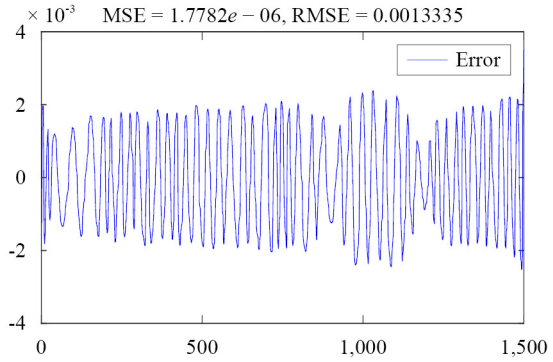
× 10^-3
MSE = 1.7782e − 06, RMSE = 0.0013335
Error

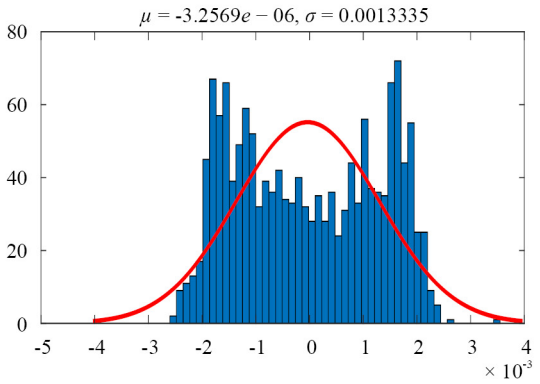
μ = -3.2569e − 06, σ = 0.0013335
× 10^-3

(d)

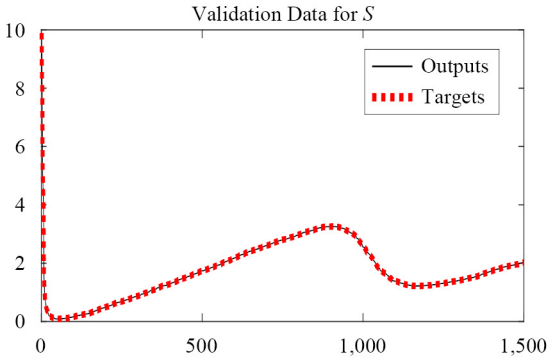
Validation Data for S
Outputs
Targets

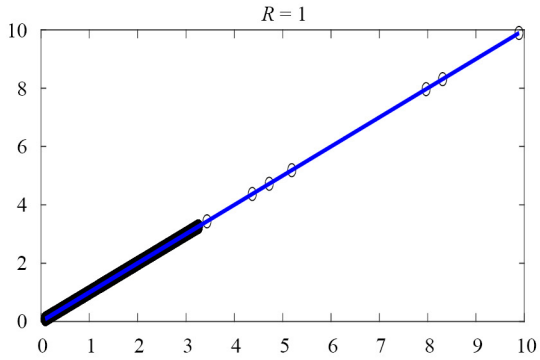
R = 1

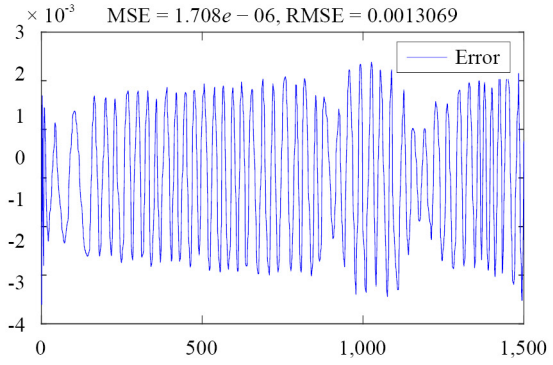
× 10^-3
MSE = 1.708e − 06, RMSE = 0.0013069
Error

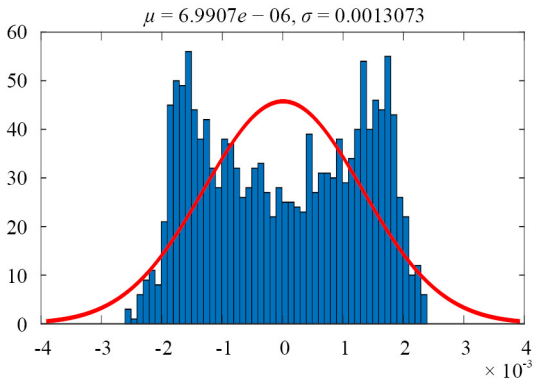
μ = 6.9907e − 06, σ = 0.0013073
× 10^-3

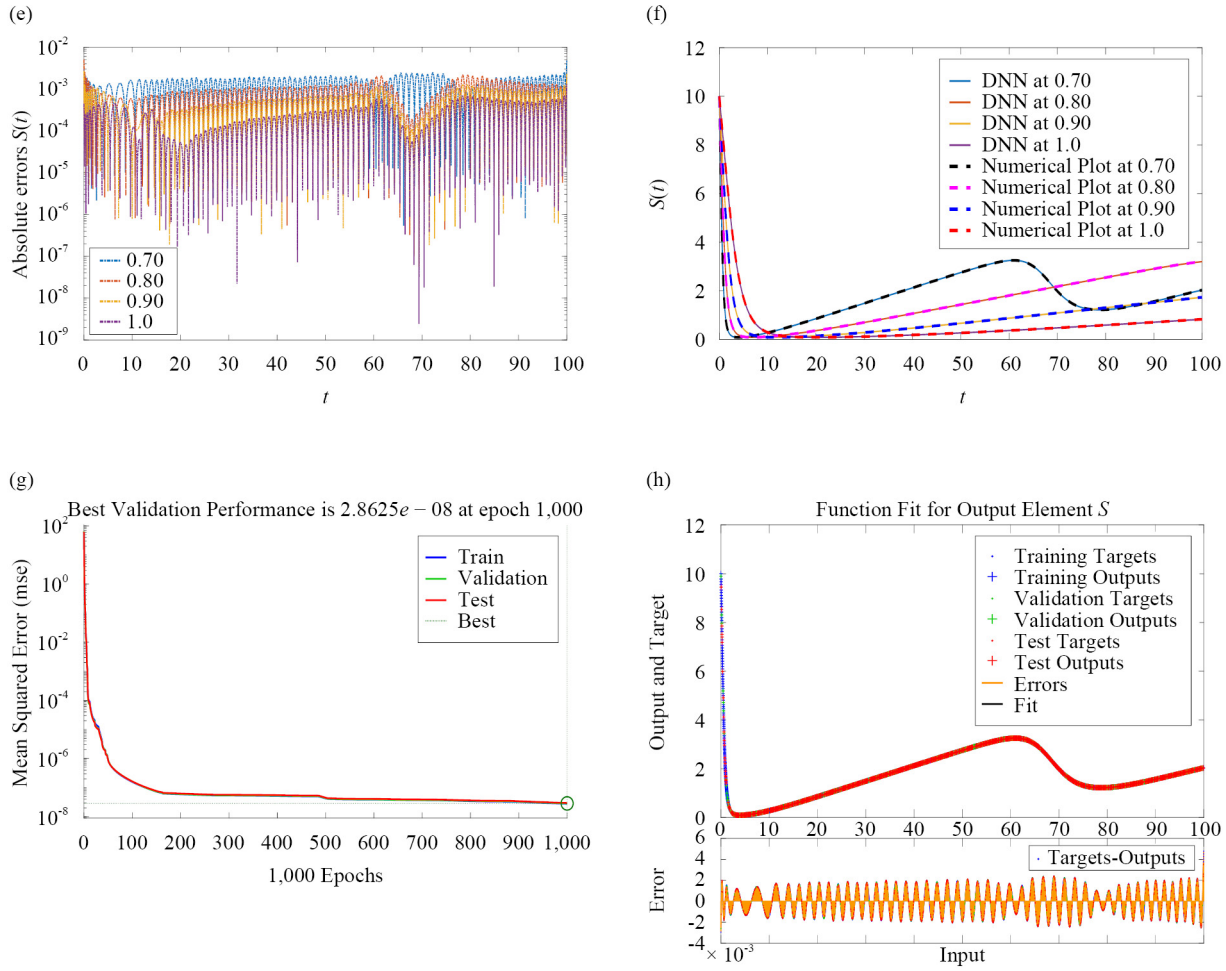

Figure 6. Graphical demonstration of susceptible class using DNNs (a) all data, (b) train data, (c) test data (d) validation of data (e) Error analysis (f) comparison of numerical results with DNNs results (g) best performance analysis (h) best validation of function fit for class S

Here, in Figure 7, we have presented various probabilistic results graphically. In sub Figure 7 (a), we have presented the MSE $= 1.5612e-06$, RMSE $= 0.0012495$ and here the regression coefficient is 1 which shows the accuracy of our simulation. In the same way in sub Figure 7 (b), the train data has been tested, where MSE $=$ MSE $= 1.5643e-06$, RMSE $= 0.0012507$. Also, in sub Figure 7 (c), and sub Figure 7 (d), we have presented the validation and test data for the infected class I. Here, MSE $= 1.5304e-06$, RMSE $= 0.0012371$ and MSE $= 1.5772e-06$, RMSE $= 0.0012559$ respectively represents the respective errors analysis of validation and test data. In sub Figures 7 (e), (f), (g) and (h), we have demonstrated the graphical presentations of absolute error analysis which is bounded by 10^{-2}, comparison between the Numerical Plot (NP) and DNN plots at various fractional order, performance and best function fit for class I. For the best validation p of class I performance is $8.2955e-08$ at epoch 100.

(a)

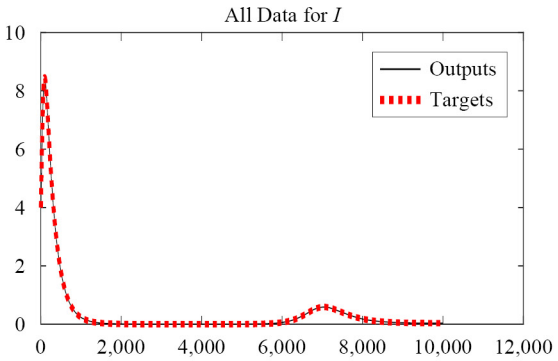
All Data for I
Outputs
Targets

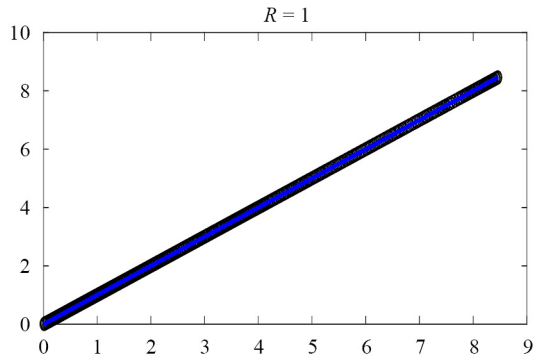
$R = 1$

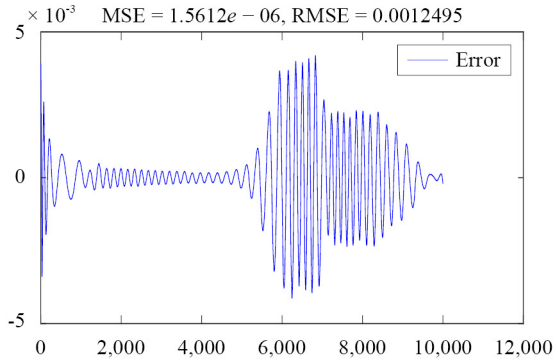
$\times 10^{-3}$ MSE = 1.5612e − 06, RMSE = 0.0012495
Error

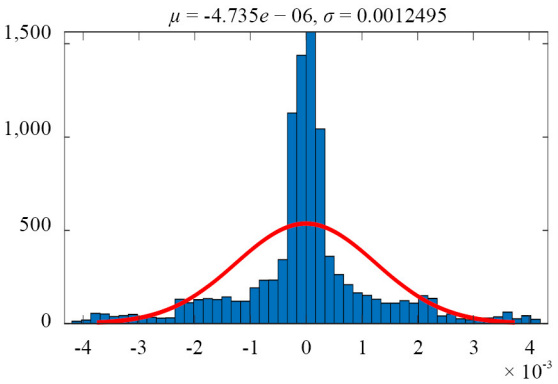
μ = -4.735e − 06, σ = 0.0012495
$\times 10^{-3}$

(b)

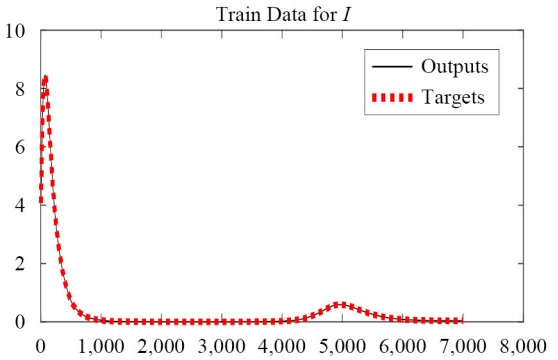
Train Data for I
Outputs
Targets

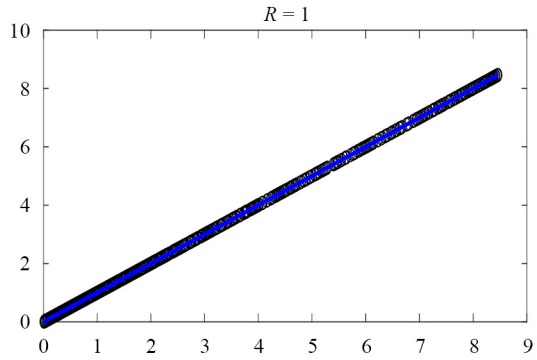
$R = 1$

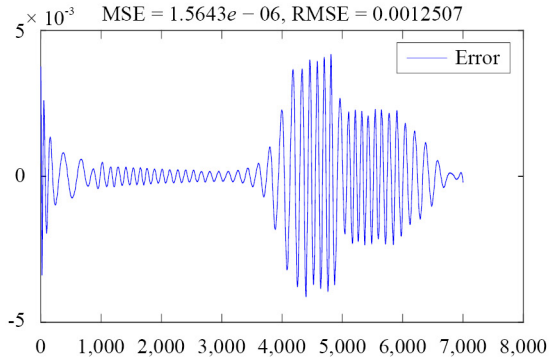
$\times 10^{-3}$ MSE = 1.5643e − 06, RMSE = 0.0012507
Error

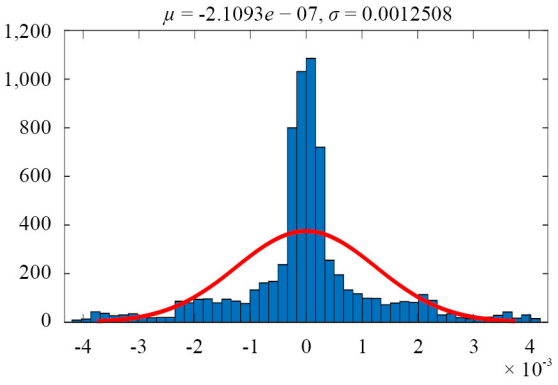
μ = -2.1093e − 07, σ = 0.0012508
$\times 10^{-3}$

(c)

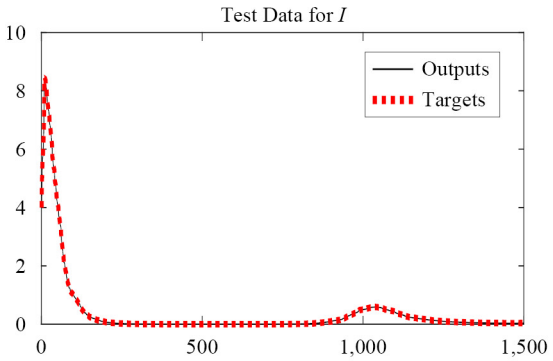
Test Data for I
Outputs
Targets

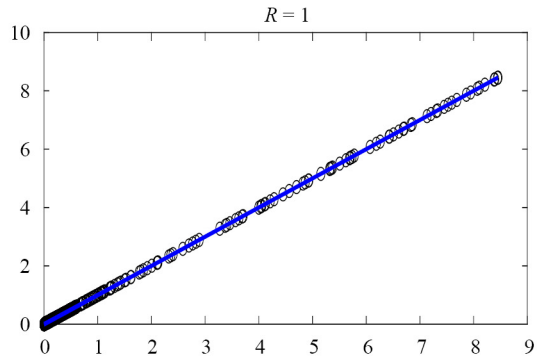
$R = 1$

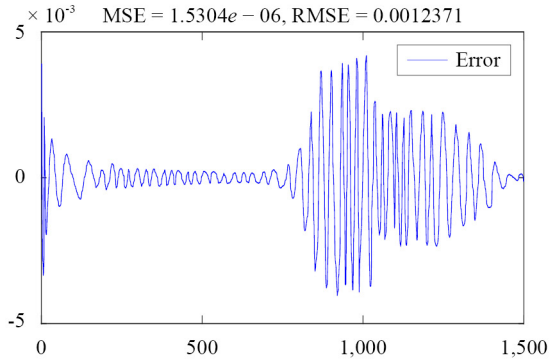
$\times 10^{-3}$ MSE = 1.5304$e-06$, RMSE = 0.0012371
Error

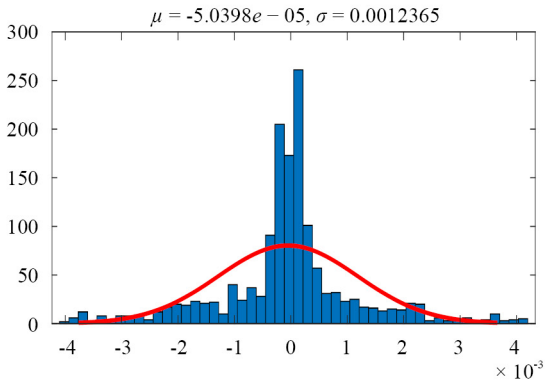
μ = -5.0398$e-05$, σ = 0.0012365
$\times 10^{-3}$

(d)

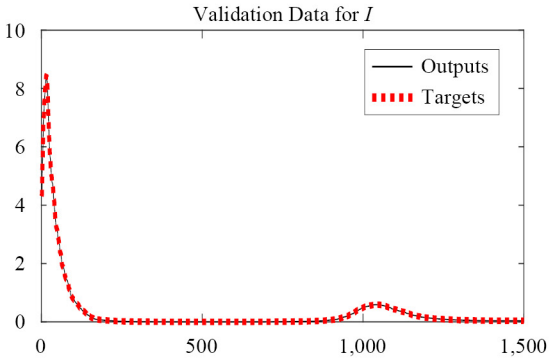
Validation Data for I
Outputs
Targets

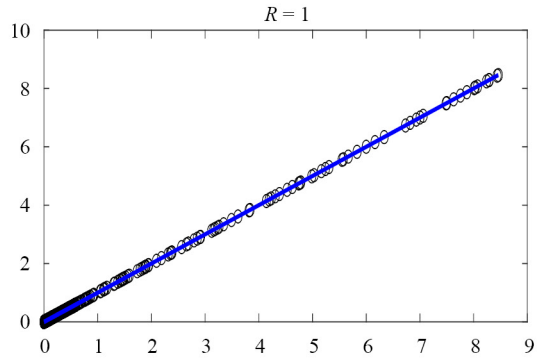
$R = 1$

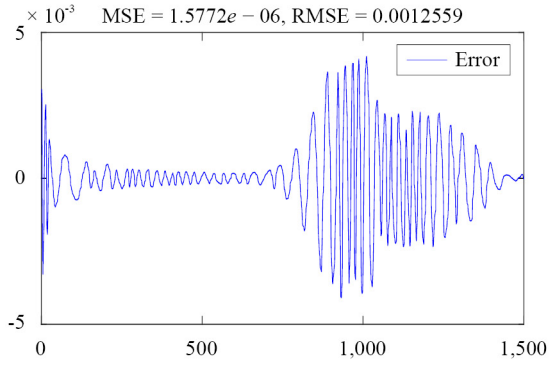
$\times 10^{-3}$ MSE = 1.5772$e-06$, RMSE = 0.0012559
Error

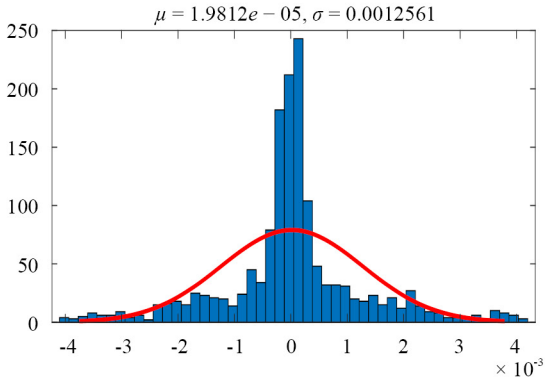
μ = 1.9812$e-05$, σ = 0.0012561
$\times 10^{-3}$

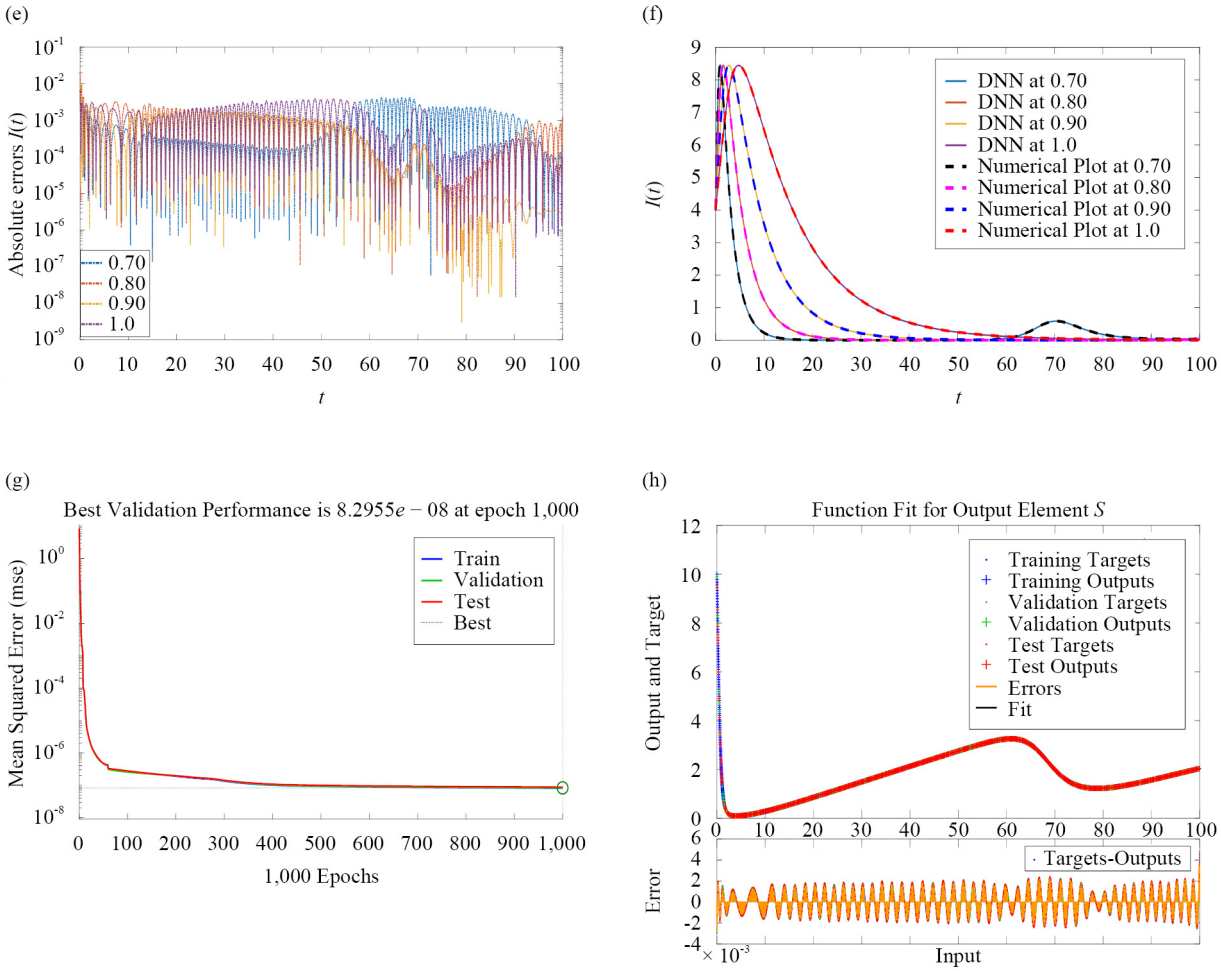

Figure 7. Graphical demonstration of infected class due to wild type virus using DNNs (a) all data, (b) train data, (c) test data (d) validation of data (e) Error analysis (f) comparison of numerical results with DNNs results (g) best performance analysis (h) best validation of function fit for class I

Here, in Figure 8, we have presented various probabilistic results graphically for the infected class due to mutant virus. In sub Figure 8 (a), we have displayed the MSE $= 3.1209e-09$, RMSE $= 5.5865e-05$ and here the regression coefficient is 1 which shows the accuracy of our simulation. Also, in sub Figure 8 (b), the train data has been presented, where MSE $= 3.2409e-09$, RMSE $= 5.6929e-05$. Also, in sub Figure 8 (c), and sub Figure 8 (d), we have displayed the validation and test data for the infected class I'. Here, MSE $= 2.6585e-09$, RMSE $= 5.1561e-05$ and MSE $= 3.0233e-09$, RMSE $= 5.4985e-05$ respectively represents the respective errors analysis of validation and test data. In sub Figures 8 (e), (f), (g) and (h), we have presented the graphical presentations of absolute error analysis which is bounded by 10^{-3}, comparison between the Numerical Plot (NP) and DNNs plots at various fractional orders, performance and best function fit for class I'. Here, we remark that the best validation performance for I' is $5.8424e-09$ at epoch 100.

(a)

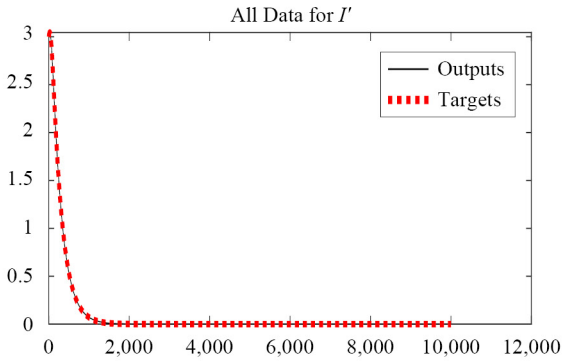
All Data for I'
Outputs
Targets

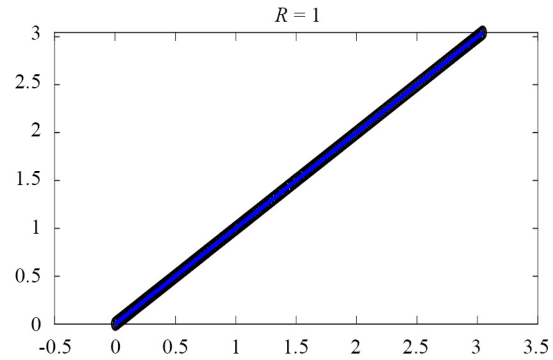
$R = 1$

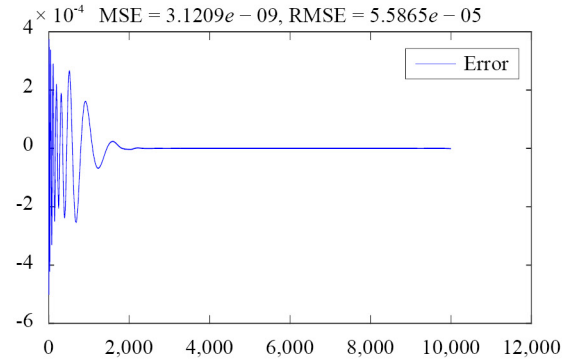
$\times 10^{-4}$ MSE = $3.1209e-09$, RMSE = $5.5865e-05$
Error

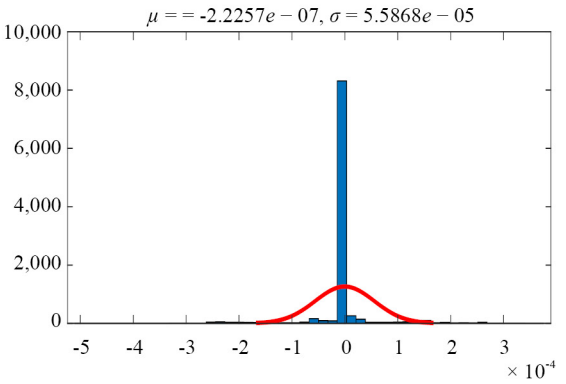
$\mu = = -2.2257e-07$, $\sigma = 5.5868e-05$
$\times 10^{-4}$

(b)

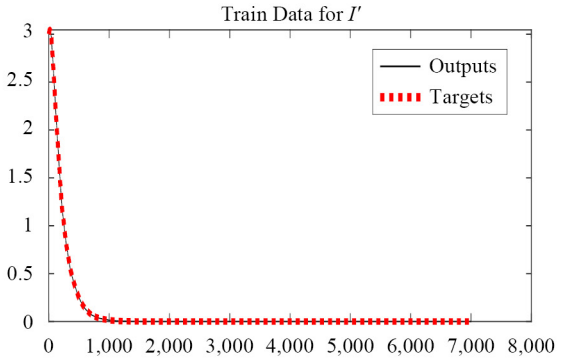
Train Data for I'
Outputs
Targets

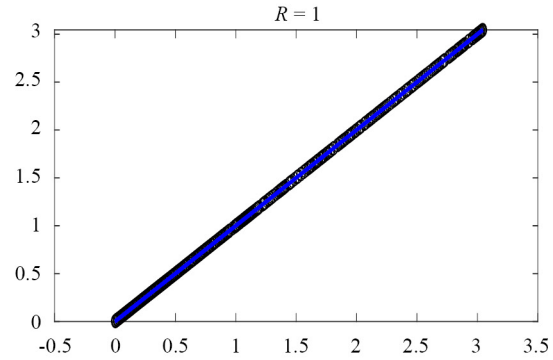
$R = 1$

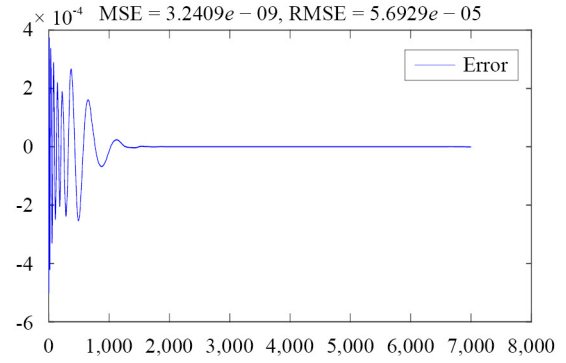
$\times 10^{-4}$ MSE = $3.2409e-09$, RMSE = $5.6929e-05$
Error

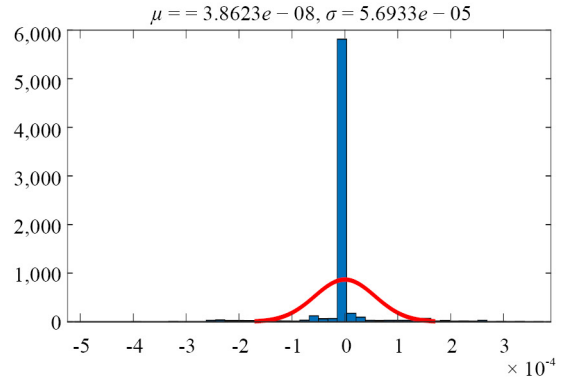
$\mu = = 3.8623e-08$, $\sigma = 5.6933e-05$
$\times 10^{-4}$

(c)

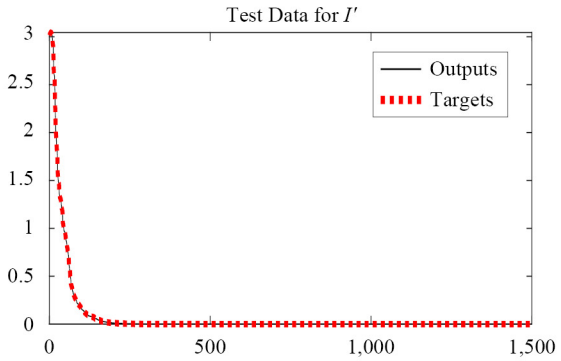
Test Data for I'
Outputs
Targets

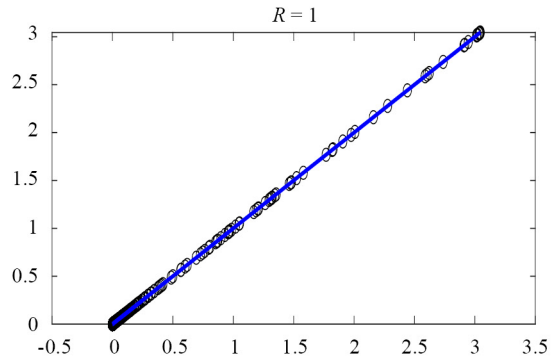
$R = 1$

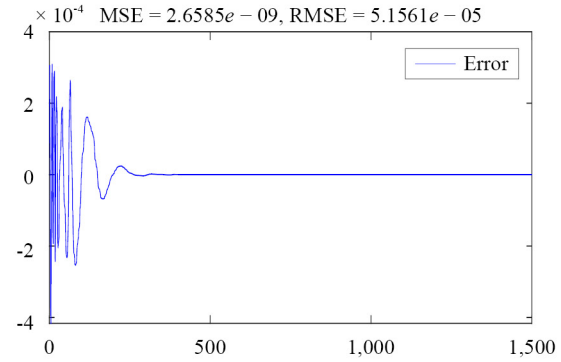
$\times 10^{-4}$ MSE = 2.6585$e-09$, RMSE = 5.1561$e-05$
Error

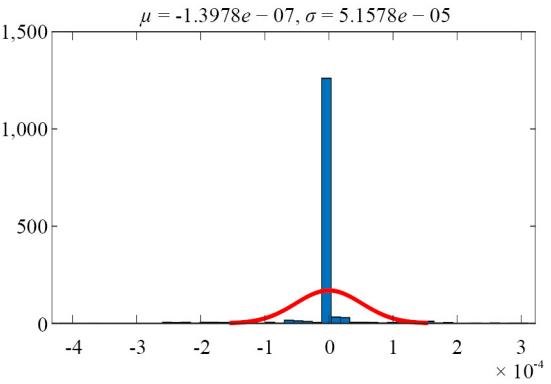
μ = -1.3978$e-07$, σ = 5.1578$e-05$
$\times 10^{-4}$

(d)

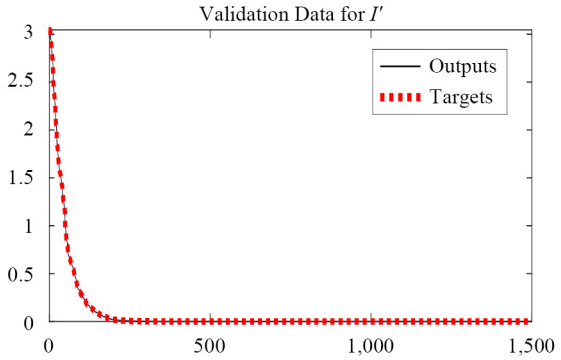
Validation Data for I'
Outputs
Targets

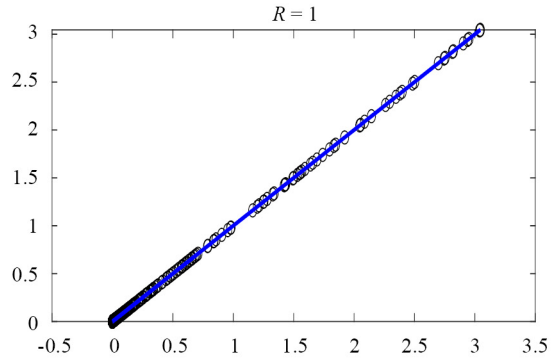
$R = 1$

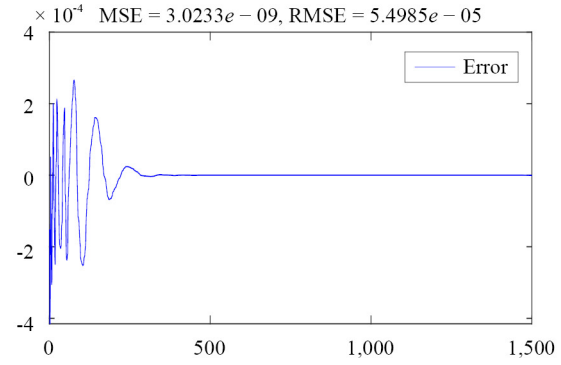
$\times 10^{-4}$ MSE = 3.0233$e-09$, RMSE = 5.4985$e-05$
Error

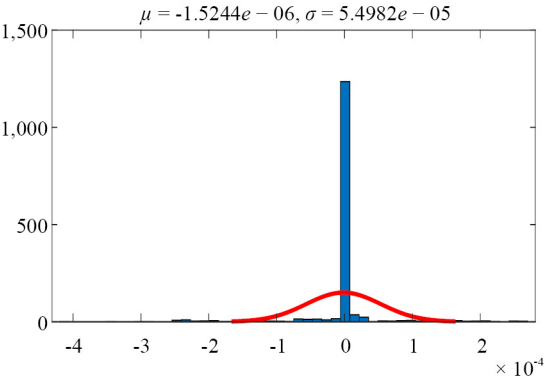
μ = -1.5244$e-06$, σ = 5.4982$e-05$
$\times 10^{-4}$

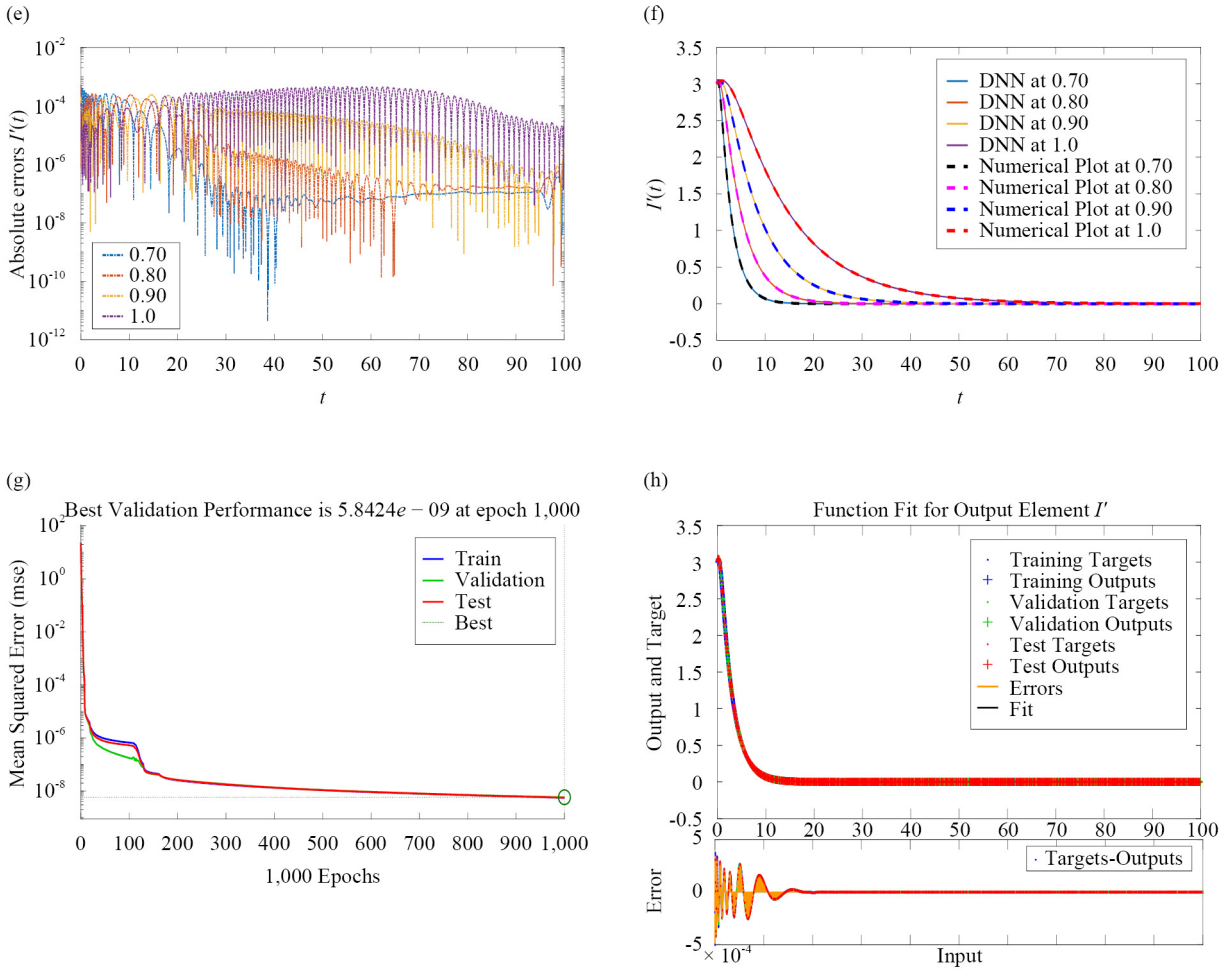

Figure 8. Graphical demonstration of infected class due to mutant type virus using DNNs (a) all data, (b) train data, (c) test data (d) validation of data (e) Error analysis (f) comparison of numerical results with DNNs results (g) best performance analysis (h) best validation of function fit for class I'

Figure 9 presents various probabilistic results graphically for the recovered class. We have displayed the MSE = $3.1209e-09$, RMSE = $5.5865e-05$ in sub Figure 9 (a) and here the regression coefficient is 1 which shows the accuracy of our simulation. Also, in sub Figure 9 (b), the train data has been presented, where MSE = $3.2409e-09$, RMSE = $5.6929e-05$. Additionally, in sub Figure 9 (c), and sub Figure 9 (d), we have displayed the validation and test data for the infected class I'. Here, MSE = $2.6585e-09$, RMSE = $5.1561e-05$ and MSE = $3.0233e-09$, RMSE = $5.4985e-05$ respectively which demonstrate the respective errors analysis of validation and test data. In sub Figures 9 (e), (f), (g) and (h), we have presented the graphical presentations of absolute error analysis which is bounded by 10^{-4}, comparison between the Numerical Plot (NP) and DNNs plots at various fractional orders, performance and best function fit for class R. The best validation performance for class R is $5.8424e-09$ at epoch 1,000.

(a)

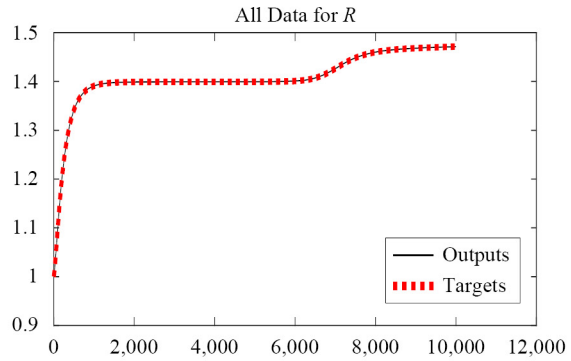
All Data for R
Outputs
Targets

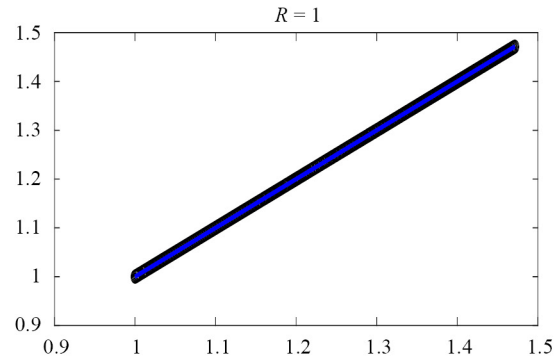
R = 1

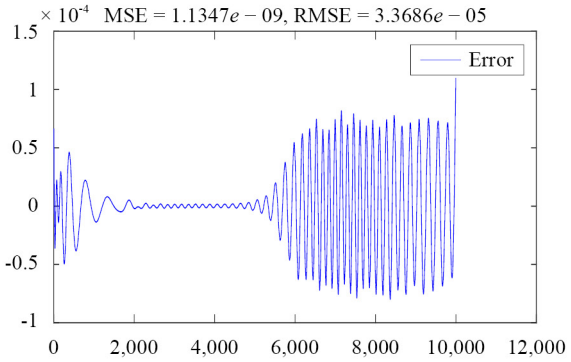
× 10^-4 MSE = 1.1347e − 09, RMSE = 3.3686e − 05
Error

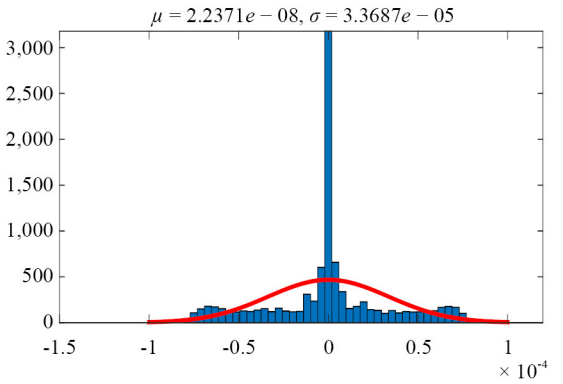
μ = 2.2371e − 08, σ = 3.3687e − 05
× 10^-4

(b)

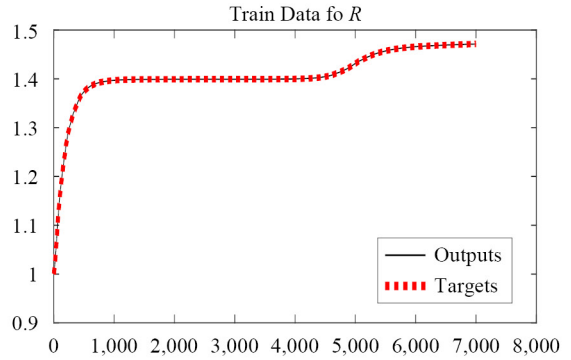
Train Data fo R
Outputs
Targets

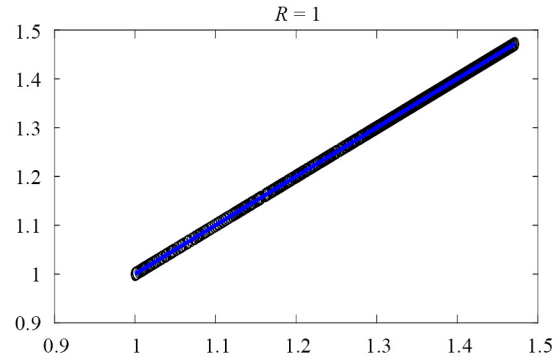
R = 1

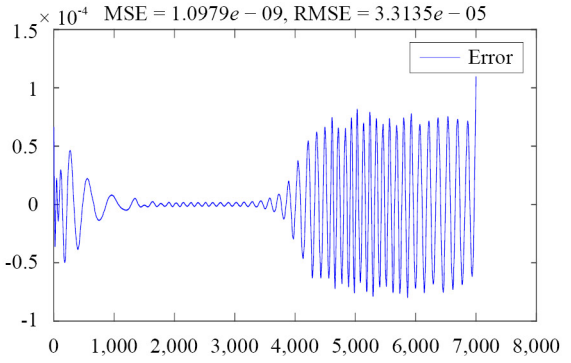
× 10^-4 MSE = 1.0979e − 09, RMSE = 3.3135e − 05
Error

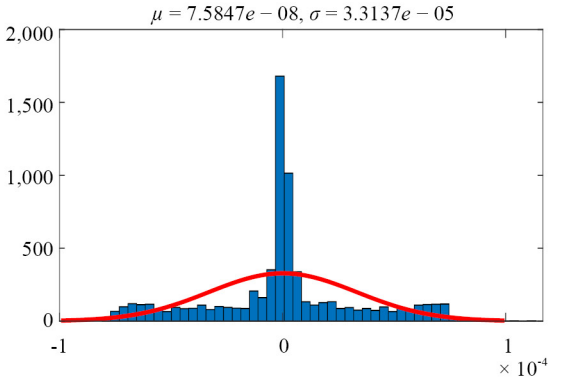
μ = 7.5847e − 08, σ = 3.3137e − 05
× 10^-4

(c)

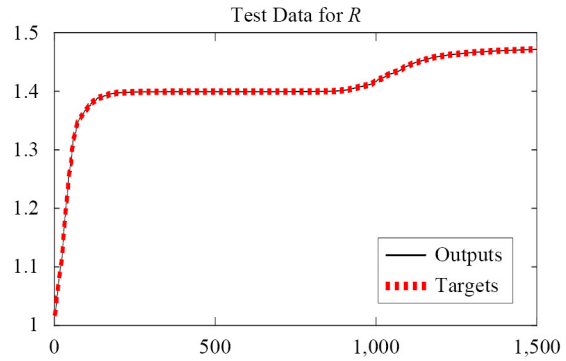
Test Data for R
Outputs
Targets

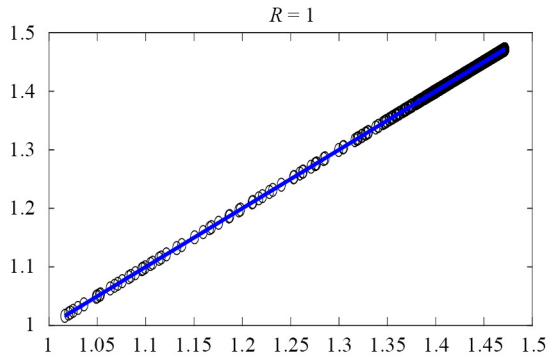
R = 1

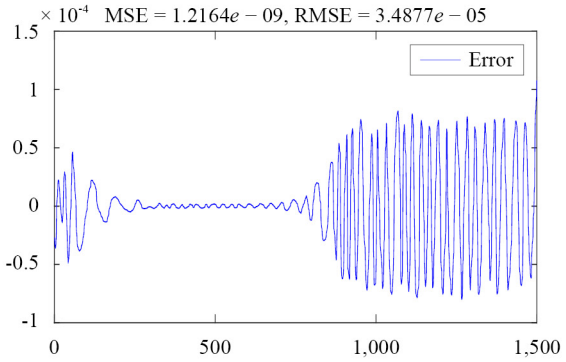
× 10^-4 MSE = 1.2164e − 09, RMSE = 3.4877e − 05
Error

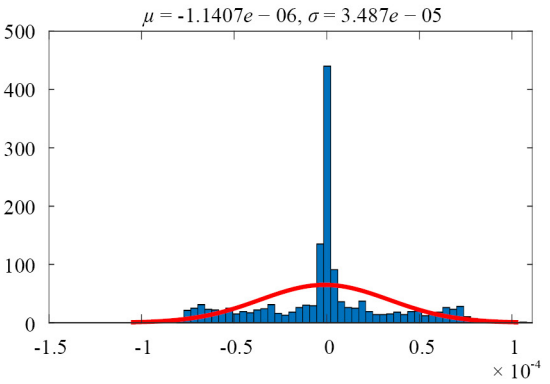
μ = -1.1407e − 06, σ = 3.487e − 05
× 10^-4

(d)

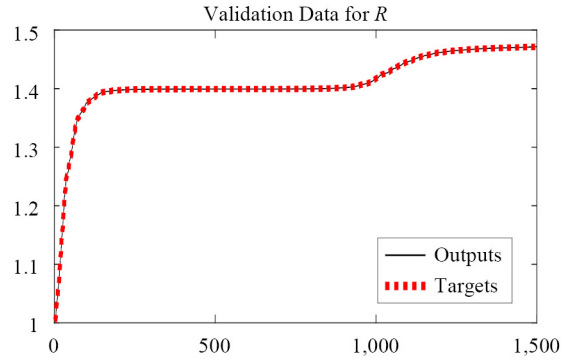
Validation Data for R
Outputs
Targets

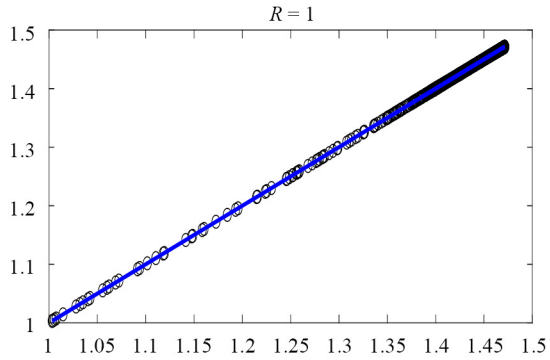
R = 1

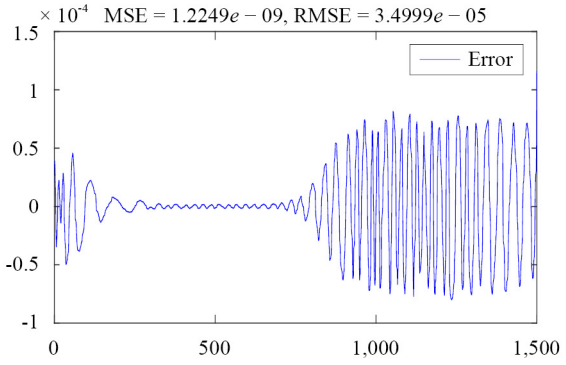
× 10^-4 MSE = 1.2249e − 09, RMSE = 3.4999e − 05
Error

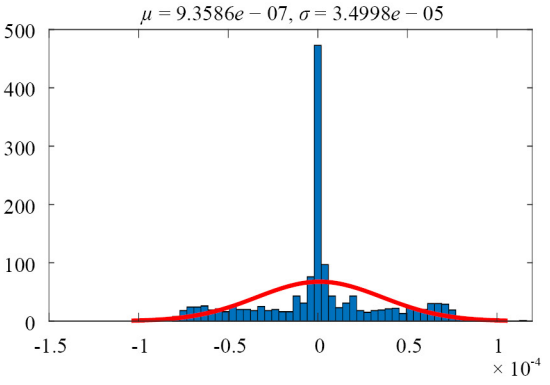
μ = 9.3586e − 07, σ = 3.4998e − 05
× 10^-4

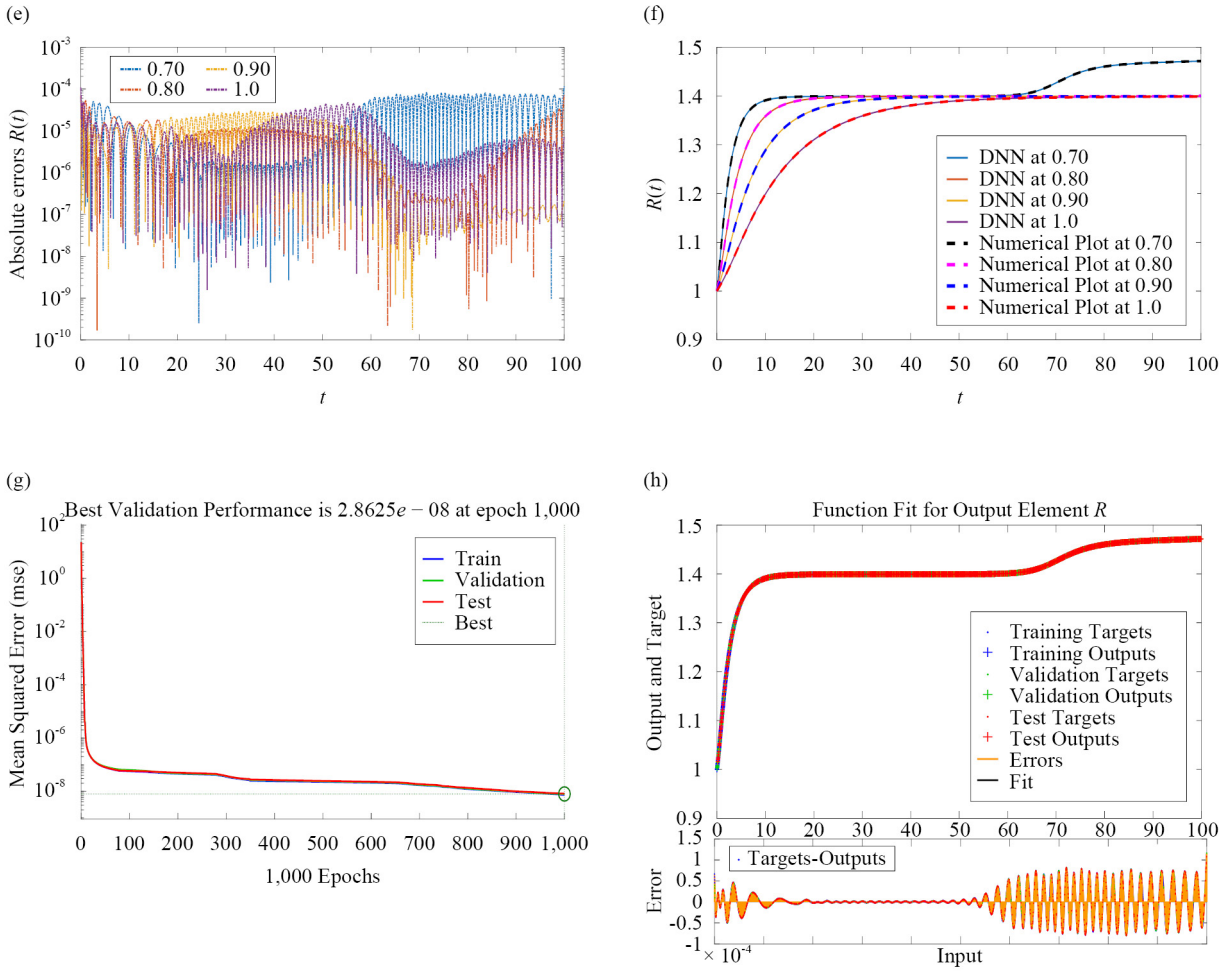

Figure 9. Graphical demonstration of recovered class due to mutant type virus using DNNs (a) all data, (b) train data, (c) test data (d) validation of data (e) Error analysis (f) comparison of numerical results with DNNs results (g) best performance analysis (h) best validation of function fit for class R

4. Conclusion

Using fractional calculus to study virus evolution model together with DNN can enhance the modeling capabilities for real world complex problems with memory dependent systems. Also, the combination of both mentioned tools increases the computational efficiency and robustness of used methodology. The fractional order system has the capabilities to address the memory and hereditary characteristic more precisely. Motivated by these outcomes, we have investigated the mentioned model by using the fractional derivative in the Liouville Caputo sense. Existence theory and numerical simulations were performed by using fixed point theory and Euler numerical method. In addition global and local stability analysis has been conducted. We have extended our study to involve DNNs to perform some computational analysis. Various results including all data, train data, test and validation of data for all compartments have been demonstrated where MSE, RMSE, and regression coefficient were presented graphically. Performance and comparison between numerical results and those due to DNNs were also presented graphically. We have presented the absolute errors for all four classes graphically. DNNs is a powerful tools which are consisted on multi hidden layers which take data through input and compile it understand its pattern and produce output. Since in data always uncertainty exists and accurate data also not always exist, therefore perfect DNN still is investigation. In the future, the mentioned tools can be used to investigate other types of models.

Authors credits

The first author updated the literature and third author drafted the paper. Third and fourth authors have edited the manuscript.

Acknowledgment

The authors would like to thank Prince Sultan University for the APC and support through the TAS research lab.

Conflict of interest

The authors declare no competing financial interest.

References

[1] Dietz K, Schenzle D. Mathematical models for infectious disease statistics. In: Atkinson AC, Fienberg SE. (eds.) *A Celebration of Statistics*. New York, NY: Springer; 1985. p.167-204.

[2] Costa A, Pires M, Resque R, Almeida SS. Mathematical modeling of the infectious diseases: key concepts and applications. *Journal of Infectious Diseases and Epidemiology*. 2021; 7(5): 209.

[3] Siettos CI, Russo L. Mathematical modeling of infectious disease dynamics. *Virulence*. 2013; 4(4): 295-306.

[4] Grassly NC, Fraser C. Mathematical models of infectious disease transmission. *Nature Reviews Microbiology*. 2008; 6(6): 477-487.

[5] Sufi F, Alsulami M. Mathematical modeling and clustering framework for cyber threat analysis across industries. *Mathematics*. 2025; 13(4): 655.

[6] Turkyilmazoglu M. Solutions to SIR/SEIR epidemic models with exponential series: numerical and non numerical approaches. *Computers in Biology and Medicine*. 2024; 183: 109294.

[7] Turkyilmazoglu M. An extended epidemic model with vaccination: weak-immune SIRVI. *Physica A: Statistical Mechanics and Its Applications*. 2022; 598: 127429.

[8] Chasnov JR. *Mathematical Biology*. California, USA; 2010.

[9] Ibeas A, Shafi M, Ishfaq M, Ali M. Vaccination controllers for SEIR epidemic models based on fractional order dynamics. *Biomedical Signal Processing and Control*. 2017; 38: 136-142.

[10] Nisar KS, Farman M, Abdel-Aty M, Ravichandran C. A review of fractional order epidemic models for life sciences problems: past, present and future. *Alexandria Engineering Journal*. 2024; 95: 283-305.

[11] Tarasov VE. Review of some promising fractional physical models. *International Journal of Modern Physics B*. 2013; 27(9): 1330005.

[12] Hassouna M, Ouhadan A. Fractional calculus: applications in rheology. In: *Fractional Order Systems*. New York: Academic Press; 2022. p.513-549.

[13] García-Aspeitia MA, Fernandez-Anaya G, Hernández-Almada A, Leon G, Magana J. Cosmology under the fractional calculus approach. *Monthly Notices of the Royal Astronomical Society*. 2022; 517(4): 4813-4826.

[14] Magin RL. Fractional calculus in bioengineering: a tool to model complex dynamics. In: *Proceedings of the 13th International Carpathian Control Conference (ICCC)*. IEEE; 2012. p.464-469.

[15] El-Amin MF. *Fractional Modeling of Fluid Flow and Transport Phenomena*. New York, United States: Elsevier and Academic Press; 2025.

[16] Abbas S, Inam I, Alharthi AM, Al-Khasawneh MAS, Az-Zobi EA, Garalleh HA. Fractional magnetohydrodynamic Casson fluid flow with thermal radiation and buoyancy effects: a constant proportional Caputo model. *Boundary Value Problems*. 2025; 2025(1): 44.

[17] Li C, Qian D, Chen Y. On Riemann-Liouville and Caputo derivatives. *Discrete Dynamics in Nature and Society*. 2011; 2011(1): 562494.

[18] Gómez JF, Torres L, Escobar RF. *Fractional Derivatives with Mittag-Leffler Kernel*. Cham, Switzerland: Springer International Publishing; 2019.
[19] Chikrii A, Matychyn I. Riemann-Liouville, Caputo, and sequential fractional derivatives in differential games. In: *Advances in Dynamic Games: Theory, Applications, and Numerical Methods for Differential and Stochastic Games*. Boston: Birkhäuser Boston; 2010. p.61-81.
[20] Samko SG, Kilbas AA, Marichev OI. *Fractional Integrals and Derivatives: Theory and Applications*. London: Taylor and Francis; 2002.
[21] Kumar K, Thakur GSM. Advanced applications of neural networks and artificial intelligence: a review. *International Journal of Information Technology and Computer Science*. 2012; 4(6): 57-68.
[22] Dande P, Samant P. Acquaintance to artificial neural networks and use of artificial intelligence as a diagnostic tool for tuberculosis: a review. *Tuberculosis*. 2018; 108: 1-9.
[23] Osipyan H, Edwards BI, Cheok AD. *Deep Neural Network Applications*. New York: CRC Press; 2022.
[24] Mohamadou Y, Halidou A, Kapen PT. A review of mathematical modeling, artificial intelligence and datasets used in the study, prediction and management of COVID-19. *Applied Intelligence*. 2020; 50(11): 3913-3925.
[25] Kraemer MU, Tsui JLH, Chang SY, Lytras S, Khurana MP, Vanderslott S, et al. Artificial intelligence for modelling infectious disease epidemics. *Nature*. 2025; 638(8051): 623-635.
[26] Khan H, Alzabut J, Almutairi DK, Alqurashi WK. The use of artificial intelligence in data analysis with error recognitions in liver transplantation in HIV-AIDS patients using modified ABC fractional order operators. *Fractal and Fractional*. 2024; 9(1): 16.
[27] Khan H, Alzabut J, Almutairi DK. Applications of artificial intelligence for clusters analysis of uranium decay via a fractional order discrete model. *Partial Differential Equations in Applied Mathematics*. 2025; 13: 101056.
[28] Khan H, Alfwzan WF, Alzabut J, Almutairi DK, Azim MA, Thinakaran R. Artificial intelligence and neural networking for an analysis of fractal-fractional Zika virus model. *Fractals*. 2025; 33(8): 1-18.
[29] Ning X, Jia L, Wei Y, Li XA, Chen F. Epi-DNNs: epidemiological priors informed deep neural networks for modeling COVID-19 dynamics. *Computers in Biology and Medicine*. 2023; 158: 106693.
[30] Timilsina M, Nováček V, D'Aquin M, Yang H. Boundary heat diffusion classifier for a semi-supervised learning in a multilayer network embedding. *Neural Networks*. 2022; 156: 205-217.
[31] Shah K, Sarwar M, Abdeljawad T. Study of fractional order epidemic compartmental model by using artificial deep neural networks. *Neural Networks*. 2025; 192: 107944.
[32] Jaiton V, Manoonpong P. Neural dynamics and synaptic plasticity in simple networks drive Lévy flight foraging and obstacle avoidance behaviors for bio-inspired autonomous flight. *Neural Networks*. 2025; 192: 107913.
[33] Siriprapaiwan S, Moore EJ, Koonprasert S. Generalized reproduction numbers, sensitivity analysis and critical immunity levels of an SEQIJR disease model with immunization and varying total population size. *Mathematics and Computers in Simulation*. 2018; 146: 70-89.
[34] Chitnis N, Hyman JM, Cushing JM. Determining important parameters in the spread of malaria through the sensitivity analysis of a mathematical model. *Bulletin of Mathematical Biology*. 2008; 70(5): 1272-1296.
[35] Wang Y, Liu J, Liu L. Viral dynamics of an HIV model with latent infection incorporating antiretroviral therapy. *Advances in Difference Equations*. 2016; 2016(1): 225.
[36] Agarwal RP, Meehan M, O'Regan D. *Fixed Point Theory and Applications*. Vol. 141. United Kingdom: Cambridge University Press; 2001.
[37] Baleanu D, Wu GC, Zeng SD. Chaos analysis and asymptotic stability of generalized Caputo fractional differential equations. *Chaos, Solitons and Fractals*. 2017; 102: 99-105.
[38] Odibat ZM, Momani S. An algorithm for the numerical solution of differential equations of fractional order. *Journal of Applied Mathematics and Informatics*. 2008; 26(1-2): 15-27.

Appendix A

Some fundamental results are given here.

Theorem 4 The solution of model (2) is bounded and lies in the given feasible region:

$$\Theta = \left\{ (S, I, I', R) \in \mathbb{R}^4_+ : \ |S+I+I'+R| \leq \frac{\Lambda}{d} \right\}.$$

Proof. Let N be the total population such that $N(t) = S(t)+I(t)+I'(t)+R(t),$ with $N(0) = N_0$ is initial population, then we have

$$\begin{aligned} {}^{C}D_t^p N(t) &= {}^{C}D_t^p[S(t)] + {}^{C}D_t^p[I(t)] + {}^{C}D_t^p[I'(t)] + {}^{C}D_t^p[R(t)] \\ &= \Lambda - dN - cI - c'I' \\ &\leq \Lambda - dN, \end{aligned} \tag{14}$$

on using Laplace transform, we have from (14)

$$s^p \mathscr{L}[N(t)] - s^{p-1}N(0) \leq \frac{\Lambda}{s} - d\mathscr{L}[N(t)],$$

which yields

$$N(t) \leq N_0 t^p \mathbb{E}_p(-dt^p) + \frac{\Lambda}{d}\mathbb{E}_p(-dt^p), \tag{15}$$

where $\mathbb{E}_p(-dt^p)$ denotes one parameter Mittag-Leffler function. In (15), when we use $t \to \infty$, we get

$$N(t) \leq \frac{\Lambda}{d}.$$

Hence the solution is bounded and lies in the given feasible region. □

Theorem 5 The solution of model (2) is positive with non-negative initial condition for all $t > 0$.

Proof. From first equation of model (2), we have

$${}^{C}D_t^p S(t) = \Lambda - dS - (\beta I + \beta' I')S > -dS,$$

on using Laplace transform, we get

$$s^p \mathscr{L}[S(t)] - s^{p-1}S(0) > -d\mathscr{L}[S(t)].$$

On solving, we get

$$S(t) > S(0)t^p \mathbb{E}_p(-dt^p) > 0, \text{ for all } t > 0,$$

hence, one has $S(t) > 0$, for all $t > 0$. With the same process, we can easily show that $I(t) > 0$, $I'(t) > 0$, and $R(t) > 0$ for all $t > 0$. □